Tectonic implications of rapid cooling of lower plate rocks from the Buckskin-Rawhide metamorphic core complex, west-central Arizona

Robert J. Scott* *Department of Earth Sciences, Monash University, Melbourne, Australia*

David A. Foster *School of Earth Sciences, La Trobe University, Melbourne, Australia* and *Department of Geology, University of Florida, Gainesville, Florida 32611*

Gordon S. Lister *Department of Earth Sciences, Monash University, Melbourne, Australia*

ABSTRACT

Lower plate rocks exposed in the Buckskin-Rawhide metamorphic core complex, west-central Arizona, underwent a pronounced increase in cooling rate 7–12 m.y. after the onset of extensional tectonic denudation at ca. 27 Ma. A detailed $^{40}Ar/^{39}Ar$ study of lower plate rocks exposed near Planet Peak, in the southwest part of the core complex, indicates that the highest-level mylonitic rocks exposed in the complex cooled below 350 °C prior to 20 ± 1 Ma, at an average rate of ≤15 °C/m.y. Thereafter, the cooling rate of these rocks increased progressively, peaking at 280–80 °C/m.y. prior to initial exposure of the core between 15.1 and 13.3 Ma. Published K-Ar, $^{40}Ar/^{39}Ar$, and fission-track ages for the most recently unroofed lower plate rocks, exposed at the northeastern end of the core complex, are consistent with a similar cooling history, although the abrupt increase in cooling rate occurred as many as 5 m.y. later in this area.

Because the increase in the cooling rate appears to have occurred progressively later toward the northeast, it is unlikely to reflect changes in slip rate. It appears to have coincided with cooling below 350–300 °C, and thus is interpreted to reflect steepening of the detachment system above the brittle-ductile transition. Thermochronological data from lower plate rocks in the Planet Peak area, together with constraints on their initial exposure at the surface, are consistent with an increase in the dip of the detachment from ≤5° at midcrustal depths (where it was represented by a shear zone) to <24° in the upper crust.

At temperatures below 200–150 °C, lower plate rocks at both ends of the core complex probably cooled at rates >130 °C/m.y., which can not be reconciled with the average dip (≤25°) and slip rate (6–12 mm/yr) for the detachment fault, given the likely geothermal gradient (~25 °C/km) during the early stages of extension. This implies that cooling did not keep pace with denudation at upper crustal levels. The very high cooling rates are interpreted to have primarily reflected the development of a pronounced thermal discontinuity across the detachment fault (possibly >100 °C), as hot lower plate rocks were transported to shallow crustal levels. Rapid cooling of the lower plate at these levels may have been enhanced by interaction with fluids derived from the upper plate, consistent with models that link the shallow-level (<2–3 km), moderate-temperature (<330 °C) hydrothermal mineralization along detachment faults to the rapid uplift of hot lower plate rocks.

INTRODUCTION

Thermochronological data from lower plate rocks in metamorphic core complexes commonly record evidence for very rapid cooling (d*T*/d*t* possibly >100 °C/m.y. [*T* = temperature, *t* = time]) during denudation (Davis, 1988; Foster et al., 1990a, 1993; Baldwin et al., 1993). Abrupt increases in cooling rate during denudation have been interpreted to reflect periods of more rapid slip on detachment systems, and thus peaks in the rate of extension (e.g., Davis, 1988). However, it is unknown whether cooling of the lower plate keeps pace with denudation (e.g., House and Hodges, 1994), thus the use of thermochronological data to infer changes in slip rate or geometry (e.g., Lee, 1995) for detachment systems is questioned. In some cases, rapid cooling may even be largely independent of denudation rate, and reflect the decay of transient thermal anomalies in and around high-level intrusions emplaced prior to and during extension (Lister and Baldwin, 1993).

Numerical modeling of the thermal consequences of slip on low-angle normal faults suggests that cooling of the footwall does not keep pace with uplift with respect to the Earth's surface, where denudation rates are >0.5–1.0 mm/yr (Ruppel et al., 1988). Accordingly, a significant perturbation (increase) of the geothermal gradient in the upper crust is expected in areas undergoing rapid denudation (e.g., Winslow et al., 1994). As a result, cooling rates for denuded rocks should increase as they approach the surface (thermal boundary layer) in response to development of a thermal discontinuity between the upper and lower plates, even if denudation rates remain relatively constant. For example, Ruppel et al. (1988, Fig. 11a, p. 955) showed that for an ambient geothermal gradient of ~10 °C/km, rocks 5 km below a detachment fault, denuded at a constant rate of 2.0 mm/yr, should be 80–90 °C hotter after uplift from 25 to 5 km than rocks denuded from the same depth at a rate of 0.5 mm/yr. Furthermore, rocks uplifted from 25 to 5 km at 2.0 mm/yr should continue to cool rapidly for several million years after denudation ceases (Ruppel et al., 1988, Fig. 11a, p. 955).

Slip rates on detachment systems associated with core complexes in the southwestern United States are typically on the order of 6–9 mm/yr (e.g., Buckskin-Rawhide: 6–9 mm/yr [Spencer and Reynolds, 1991; Foster et al., 1993; this study], Whipple: 7–8 mm/yr [Davis, 1988; Foster et al., 1994]; and Chemehuevi: 7.7 mm/yr [John and Foster, 1993]). Although field studies suggest

*Present address: Centre for Ore Deposit Research SRC, University of Tasmania, GPO Box 252-79 Hobart, Tasmania, Australia 7001; e-mail: robert.scott@utas.edu.au

Data Repository item 9820 contains additional material related to this article.

GSA Bulletin; May 1998; v. 110; no. 5; p. 588–614; 15 figures; 5 tables.

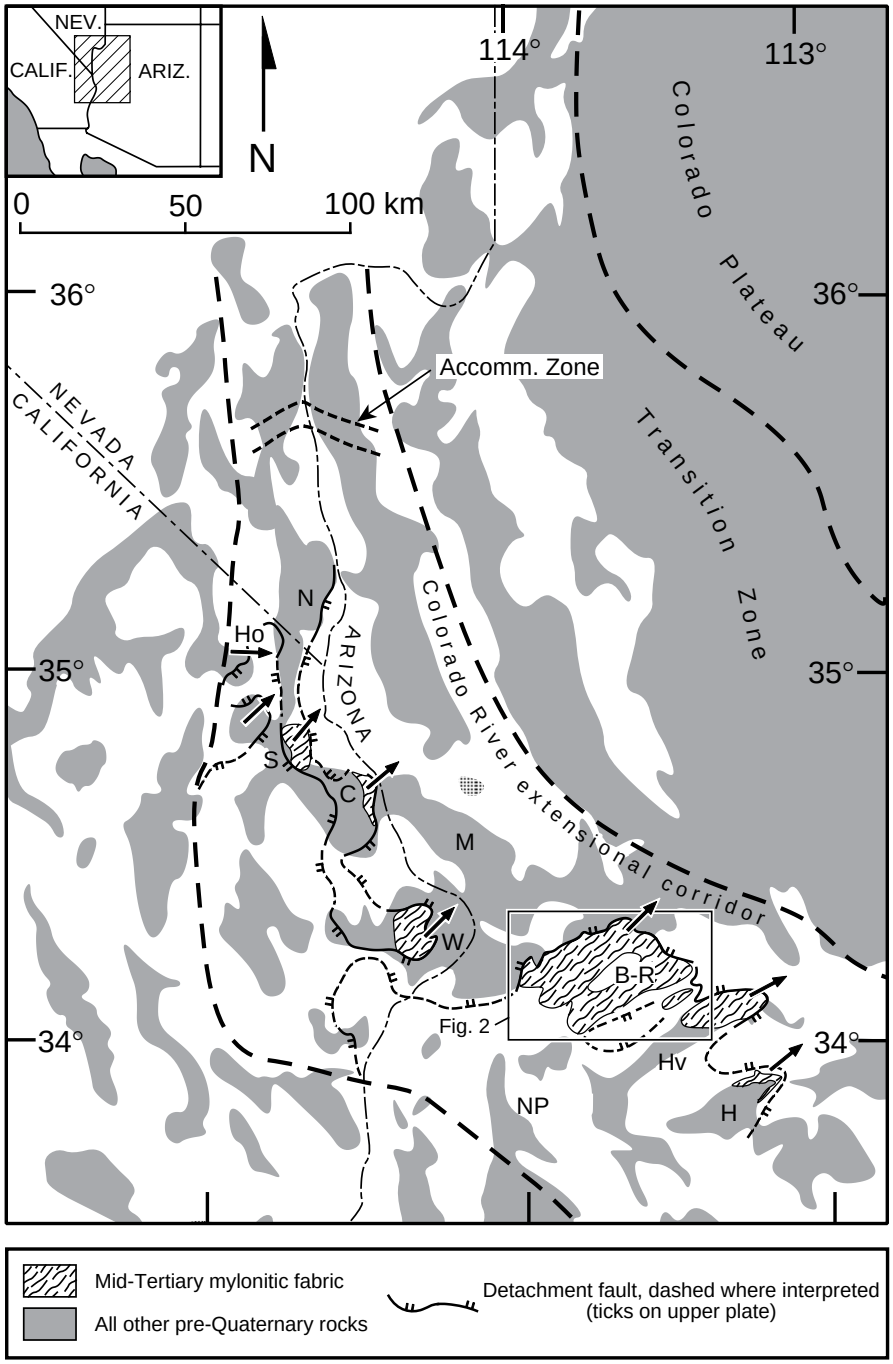

Figure 1. Simplified map showing the location of core complexes, major detachment faults, and the areal extent of Tertiary mylonites within the Colorado River extensional corridor. Regions northeast and southwest of the corridor underwent minor extension at upper crustal levels during Tertiary time. Heavy arrows indicate displacement directions on the detachment systems. The accommodation zone at the northern end of the extensional corridor marks a transition from top-to-the-northeast to top-to-the-southwest displacement on the dominant fault systems at upper crustal levels (Faulds et al., 1990; Faulds, 1992). From north to south the core complexes are: S—Sacramento, C—Chemehuevi, W—Whipple, B-R—Buckskin-Rawhide, Hv—Harcuvar, and H—Harquahala. Detachment faults in the Homer (Ho) and Newberry (N) mountains are transitional to smaller displacement normal fault systems at the northern end of the extensional corridor. Thermochronological data from tilted crustal sections exposed in the Mohave (M) and northern Plomosa (NP) Mountains indicate that the geothermal gradient at the southern end of the corridor could have been as low as 20–25 °C/km during the early stages of extension (Foster et al., 1994).

that the detachment faults were active at very low dips (<25°: John, 1987; Davis and Lister, 1988; Scott and Lister, 1992; Livaccari et al., 1993; John and Foster, 1993), these slip rates equate to denudation rates >2 mm/yr, suggesting that significant perturbation of the geothermal gradient should have occurred.

Despite theoretical predictions about thermal effects of rapid denudation, few field-based studies have examined the relation between slip and cooling rates during core-complex development. One exception is the study by House and Hodges (1994), who argued that rapid cooling of the lower plate of the Bitterroot metamorphic core complex (Idaho-Montana) largely postdated tectonic unroofing. However, the $^{40}Ar/^{39}Ar$ data for K-feldspar, muscovite, and biotite used in this study only demonstrate that rapid cooling postdated mylonitization, not necessarily the continued denudation of the lower plate at higher crustal levels (Foster, 1995). Furthermore, it is difficult to evaluate the significance of changes in cooling rate at a single location in the lower plate (see House and Hodges, 1994), as these could be either temporally or spatially controlled. Temporally controlled changes may reflect changes in slip rate on the detachment system or cooling following pluton emplacement, while the spatially controlled changes could reflect the thermal structure of the crust, the geometry of the detachment system, or both. Ideally, thermochronological data from along the length of a core complex (parallel to the slip direction)

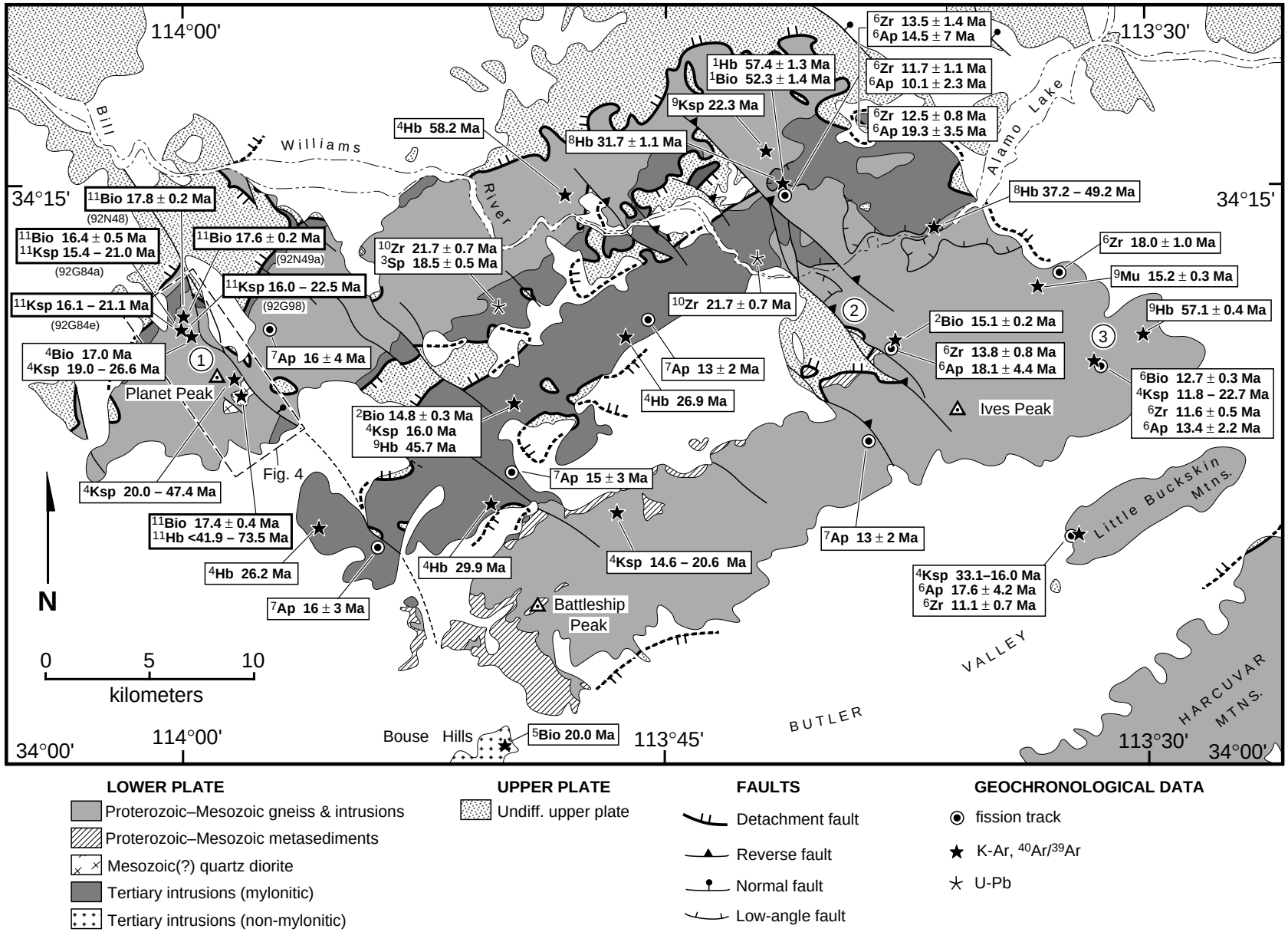

Figure 2. Summary of geochronological data for lower plate rocks from the Buckskin-Rawhide metamorphic core complex. Sources of data and methods of analysis denoted by superscripts: 1—K-Ar, Shackelford (1980); 2—K-Ar, Spencer et al. (1989a); 3—U-Pb, Bryant and Wooden (1989); 4—$^{40}Ar/^{39}Ar$, Richard et al. (1990); 5—K-Ar (sample location approximate); Spencer and Reynolds (1990); 6—Fission track, Bryant et al. (1991); 7—Fission track, Foster et al. (1993); 8—$^{40}Ar/^{39}Ar$, Scott (1995); 9—Fryxell *in* Bryant (1995); 10—Wooden *in* Bryant (1995); and 11—$^{40}Ar/^{39}Ar$, this study. Circled numbers 1, 2, and 3 denote the locations used to constrain cooling history of the lower plate (see Fig. 12). The study area (Fig. 4) is at the southwestern end of the Planet Peak arch (Bryant and Wooden, 1989), the northernmost of three northeast-trending lower plate ridges. The Bill Williams River separates the Buckskin (south) and Rawhide (north) Mountains, although the two ranges are geologically continuous. Map is compiled from Bryant (1995) and Spencer (1989).

are required in order to reliably interpret the physical significance of variations in cooling rate at a single location (Foster, 1995).

We have combined a detailed $^{40}Ar/^{39}Ar$ study of lower plate rocks at the southwestern end of the Buckskin-Rawhide metamorphic core complex with previously published thermochronological data from elsewhere in the complex in order to examine the cooling history of the lower plate during Miocene denudation. Lower plate rocks at both ends of the core complex record a similar greater than 10 fold increase in cooling rate during denudation. This is interpreted to reflect both the ramped geometry of the detachment system and the thermal structure of the upper crust during, and as a result of, extension. The lower plate appears to have retained much of its heat during rapid transport to shallow crustal levels, undergoing extremely rapid cooling ($dT/dt > 130$ °C/m.y.) within a few kilometers of the surface. Our interpretation supports earlier models that have linked moderate temperature (i.e., ≤330 °C), but very shallow level, Fe-Cu mineralization along detachment faults to the rapid denudation of hot lower plate rocks (e.g., Spencer and Welty, 1986; Roddy et al., 1988).

Geological Setting of the Buckskin-Rawhide Mountains

The Buckskin-Rawhide metamorphic core complex is the largest of six metamorphic core complexes exposed in the Colorado River extensional corridor, a 50–125-km-wide belt that underwent extreme crustal extension during latest Oligocene and Miocene time (Fig. 1; Howard and John, 1987). The core complexes are exposed along the axis of the corridor, south of lat 35°N, where the greatest extension occurred (locally ≥400%, e.g., Spencer and Reynolds, 1991). Unroofing of the core complexes was accomplished along originally northeast-dipping detachment systems, rooted beneath the western margin of the transition zone (Howard and John, 1987; Davis and Lister, 1988; Spencer and Reynolds, 1991). Spencer and Reynolds (1989, 1991) estimated that a total of 55–75 km top-to-the-northeast displacement occurred on the Buckskin-Rawhide fault system in early and middle Miocene time.

The lower plate of the Buckskin-Rawhide metamorphic core complex is exposed in three northeast-trending ridges, which reflect the corrugated form of the now largely eroded (but originally overlying) detachment fault system (Fig. 2, Shackelford, 1980; Rehrig and Reynolds, 1980; Spencer and Reynolds, 1989). The detachment fault and thin remnants of the upper plate are best preserved in broad shallow synforms between the lower plate arches, and along the northeastern and northwestern flanks of the core complex (Fig. 2). Locally, hydrothermal Cu + Fe mineralization (T<330 °C) occurs along the detachment fault, and within adjacent rocks in the upper and lower plates (Spencer and Welty, 1986; Roddy et al., 1988).

The lower plate is dominated by Early Proterozoic to Cretaceous layered migmatitic gneiss, intruded by a variety of Early Proterozoic to Tertiary plutonic rocks (Bryant and Wooden, 1989; Bryant, 1995; Bryant et al., 1996). In areas not as strongly affected by subsequent deformation events, particularly the southern and southwestern parts of the core complex, Proterozoic rocks locally preserve a well developed, steeply dipping, northeast-trending gneissic fabric (Scott, 1995). The fabric is defined by upper amphibolite facies mineral assemblages and may have formed during the 1.7 Ga Ivanpah orogeny (e.g., Bennett and DePaolo, 1987; Wooden and Miller, 1990). However, as a similarly oriented, but more weakly developed "gneissic" fabric overprints a Mesozoic(?) intrusion near Planet Peak (see Sample 92C81, Appendix 1), the steeply dipping fabric in the Proterozoic rocks may have a more complex origin. The gneisses were intruded by Early or Middle Proterozoic granite and granodiorite, Jurassic diorite and gabbro and Cretaceous granite (Bryant and Wooden, 1989; Bryant, 1995).

Numerous slivers of metasedimentary rock including calc-silicate, marble, quartzite, and feldspathic schist are intercalated with Proterozoic gneisses in the lower plate (Bryant and Wooden, 1989; Spencer and Reynolds, 1989). These rocks generally crop out as lenses a few meters thick with lateral extents of 10s to 100s of meters. However near Battleship Peak, in the southernmost part of the Buckskin Mountains, the metasedimentary sequence is up to 800 m thick and forms the structurally highest unit in the lower plate (Fig. 2; Marshak and Vander Muelen, 1989; Bryant and Wooden, 1989). The metasedimentary rocks are thought to be slivers of the Paleozoic-Mesozoic shelf succession, incorporated into the basement during deep-seated thrusting in the late Mesozoic (Bryant and Wooden, 1989; Spencer and Reynolds, 1989). In much of southern and western Arizona (including the Buckskin-Rawhide Mountains) and southeastern California, the late Mesozoic compressional deformation was accompanied by regional metamorphism grading to upper amphibolite facies (locally associated with migmatization) and widespread emplacement of peraluminous and metaluminous intrusions (Reynolds et al., 1988; Knapp and Heizler, 1990; Foster et al., 1990a; 1992; Bryant, 1995). Late Cretaceous to early Tertiary K-Ar and $^{40}Ar/^{39}Ar$ cooling ages for hornblende from lower plate gneisses exposed in the northeast of the Buckskin-Rawhide core complex (Shackelford, 1980; Richard et al., 1990; Bryant, 1995) indicate that at least the deepest exposed portions of the lower plate remained above 500 °C until the early Tertiary. A 52.3 ± 1.4 Ma K-Ar age for a biotite sample from the lower plate in the Rawhide Mountains (Fig. 2; Shackelford, 1980) implies rapid cooling to below ~300 °C during the early Tertiary. However, this cooling age is inconsistent with other thermochronological data from the core complex and is considered spurious (for further discussion see Bryant et al., 1991, p. 12,378).

Nearly 30% (>200 km^2) of the exposed lower plate in the Buckskin-Rawhide Mountains consists of metaluminous to weakly peraluminous mafic to felsic intrusions (Swansea Plutonic Suite) emplaced immediately prior to or during the early stages of core complex formation (Fig. 2; Bryant and Wooden, 1989; Richard et al., 1990; Bryant et al., 1993; Bryant, 1995). The suite includes medium to coarse-grained gabbro, diorite, quartz diorite, granodiorite and granite (Bryant and Wooden, 1989; Bryant, 1995). U-Pb analyses of zircon splits from widely separated felsic and mafic members of the suite both lie on a chord with a lower intercept of 21.7 ± 0.7 Ma (Fig. 2; Bryant, 1995; Bryant et al., 1996). $^{40}Ar/^{39}Ar$ plateau ages for hornblende from three other mafic intrusions in the suite range from 29.9 to 26.2 Ma, with age spectra consistent with minimal contamination with excess argon (Fig. 2; Richard et al., 1990). A hornblende sample from the Swansea Plutonic Suite in the central Buckskin Mountains (possibly a wall-rock inclusion, e.g., Bryant, 1995) yielded an anomalously old $^{40}Ar/^{39}Ar$ total gas age of 45.7 Ma (Fig. 2; Fryxell *in* Bryant, 1995). Numerous thin (≤5 m), consistently oriented sheet-like intrusions also occur throughout the lower plate, particularly in the Planet Peak (Scott, 1995) and Battleship Peak (Bryant, 1995) areas, at the southwestern end of the core complex. They are generally very fine grained and porphyritic, and range from mafic to felsic-intermediate in composition. The sheet-like intrusions cut the Swansea Plutonic Suite northwest of Planet Peak, indicating they are latest Oligocene to Miocene in age. Similar intrusions in the neighboring Whipple Mountains were dated at 26 ± 5 Ma (U-Pb zircon, Wright et al., 1986) and 24.1 ± 6.6 Ma (U-Pb zircon, Foster, unpublished data).

Most lower plate rocks in the Buckskin-Rawhide Mountains, including the Swansea Plutonic suite and the thin sheet-like intrusions, are at least weakly overprinted by a moderately to gently dipping mylonitic fabric formed under biotite-

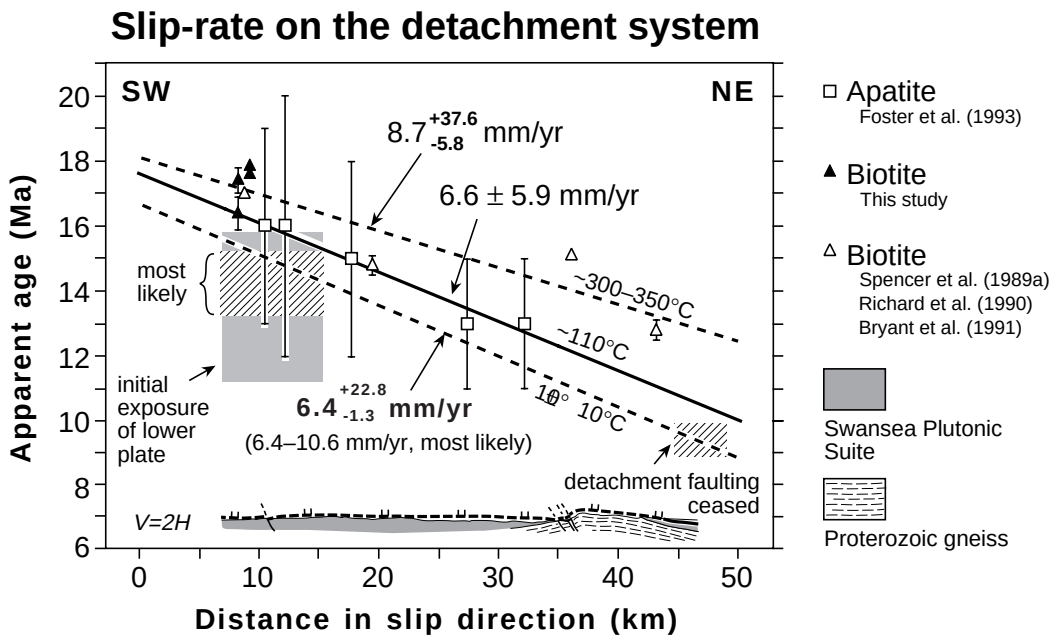

Figure 3. Apparent age of biotite (K-Ar and $^{40}Ar/^{39}Ar$) and apatite (fission track) vs. distance in the displacement direction of the Buckskin-Rawhide detachment system. Data are shown relative to a longitudinal section through the central arch of the core complex. The apparent 1–2 m.y. difference in cooling ages for biotite and apatite along the length of the core complex suggests that cooling rates generally exceeded 100 °C/m.y. during the latter stages of denudation. The irregular northeastward decrease in biotite age, interpreted to reflect cooling below ~300–350 °C during top-to-the-northeast displacement on the detachment system, provides little constraint on the average slip rate. The more linear decrease in apatite fission-track age toward the northeast suggests an average slip rate of 6.6 ± 5.9 mm/yr after 16 Ma. Apatite fission-track data from Bryant et al. (1991) were not used in the slip rate calculation due to the low number of grains measured for each sample and because the samples generally yielded older ages than minerals with higher closure temperatures from the same sample (see Fig. 2). Initial exposure of the lower plate at the southwestern (15.1–13.3 Ma) and northeastern ends (9.6 ± 0.3 Ma) of the core complex suggests an average slip rate of 6.4–10.6 mm/yr on the detachment fault (see text for further discussion).

grade greenschist facies conditions (Shackelford, 1980; Woodward and Osborne, 1980; Spencer and Reynolds, 1989) during Oligo-Miocene extension (Bryant and Wooden, 1989; Richard et al., 1990). Although the orientation of the mylonitic fabrics is highly variable, the mylonitic (extension) lineation consistently trends northeast, subparallel to the displacement direction on the detachment fault (Spencer and Reynolds, 1989; 1991). The mylonites predominantly record top-to-the-northeast shear, consistent with southwestward displacement of the lower plate from beneath the western margin of the Transition Zone (Fig. 1; Howard and John, 1987; Spencer and Reynolds, 1991). The mylonitic fabric is more pervasively developed toward the northeast, consistent with the unroofing of deeper (pre-extensional) structural levels in this direction (Bryant and Wooden, 1989; Spencer and Reynolds, 1989; 1991). However, there is little variation in the peak metamorphic grade of the mylonitic fabrics across the range, implying the shear zone originally had a gentle dip at midcrustal depths (Spencer and Reynolds, 1991).

The upper plate is dominated by sedimentary and volcanic rocks deposited during development of the core complex. The oldest synextensional deposits rest unconformably on either Proterozoic crystalline basement or remnants of the Mesozoic plus or minus Paleozoic cover sequence and consist chiefly of lacustrine sedimentary rocks, minor tuff and evaporites and sparse coarse clastic deposits (Spencer and Reynolds, 1989; Spencer et al., 1989b; Yarnold, 1994). These deposits record minor differential tilt (~5°) during deposition, reflecting the initial subsidence associated with down-warping (Lucchitta and Suneson, 1993; 1996) or movement on basin-bounding normal faults (Spencer et al., 1989b; Yarnold, 1994). There are few reliable constraints on the age of the oldest synextensional deposits. Generally, 23–24 Ma has been favored for the onset of extensional deformation in the southern and central parts of the CRec (e.g., Foster et al., 1993; Spencer and Reynolds, 1994; Nielson and Beratan, 1995). However, nearly concordant $^{40}Ar/^{39}Ar$ ages for biotite (26.57 ± 0.15 Ma) and K-feldspar (26.28 ± 0.01 Ma) from a tuff near the base of the synextensional sequence just north of the Rawhide Mountains (G. H. Curtis *in* Lucchitta and Suneson, 1994) appear to provide the most reliable constraint on the maximum age of the succession and indicate extension was under way by ~27 Ma. Detachment faulting at the northeastern end of the Buckskin-Rawhide Mountains continued until at least 9.6 ± 0.3 Ma (K-Ar whole-rock, Shackelford, 1980), based on the age of a locally faulted but gently dipping basalt flow overlying, or intercalated with, the uppermost part of the synextensional succession in the Artillery Mountains (Fig. 3).

At a relatively late stage during extension, clasts of mylonite and chloritic breccia were incorporated into synextensional deposits at the northeastern flank of the core complex, recording initial subareal exposure of the lower plate (Spencer and Reynolds, 1989; Yarnold, 1994). Typically, 20%–40% of clasts in the Sandtrap Conglomerate (the youngest synextensional unit) were derived from the lower plate. The underlying Chapin Wash Formation contains <5% lower plate detritus (Spencer and Reynolds, 1989; Spencer et al., 1989b). Consistent northeast-directed paleocurrents from the Sandtrap

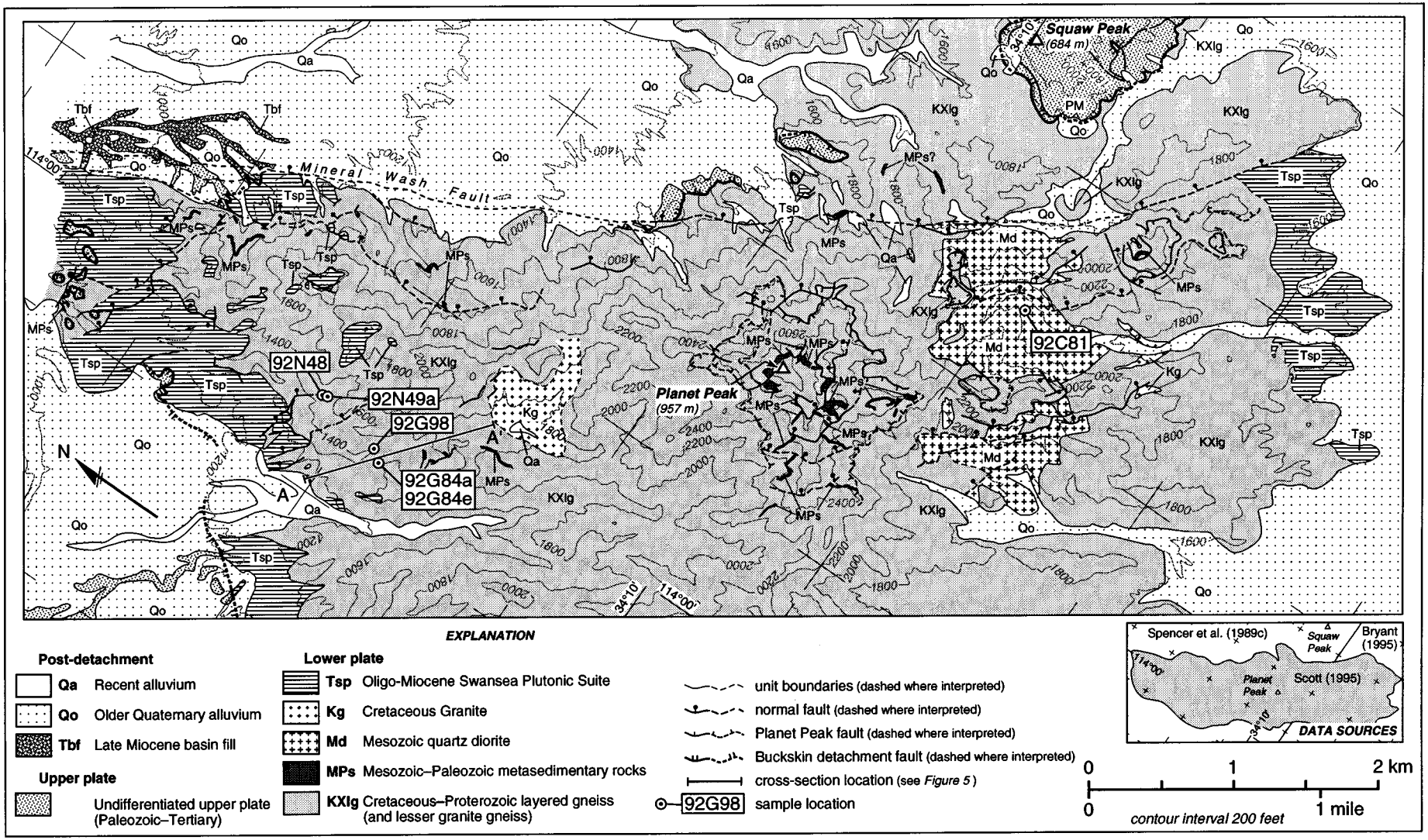

Figure 4. Geological map of the Planet Peak area showing the locations of the $^{40}Ar/^{39}Ar$ samples discussed in the text and the position of cross section A–A′ (Fig. 5). Strongly mylonitized intrusions of the Swansea Plutonic Suite locally underlie the detachment fault, or inferred position of the detachment fault, along both flanks of the Planet Peak arch, and represent the structurally highest unit in the lower plate in this area. Map is compiled from Scott (1995), Spencer et al. (1989c), and Bryant (1995).

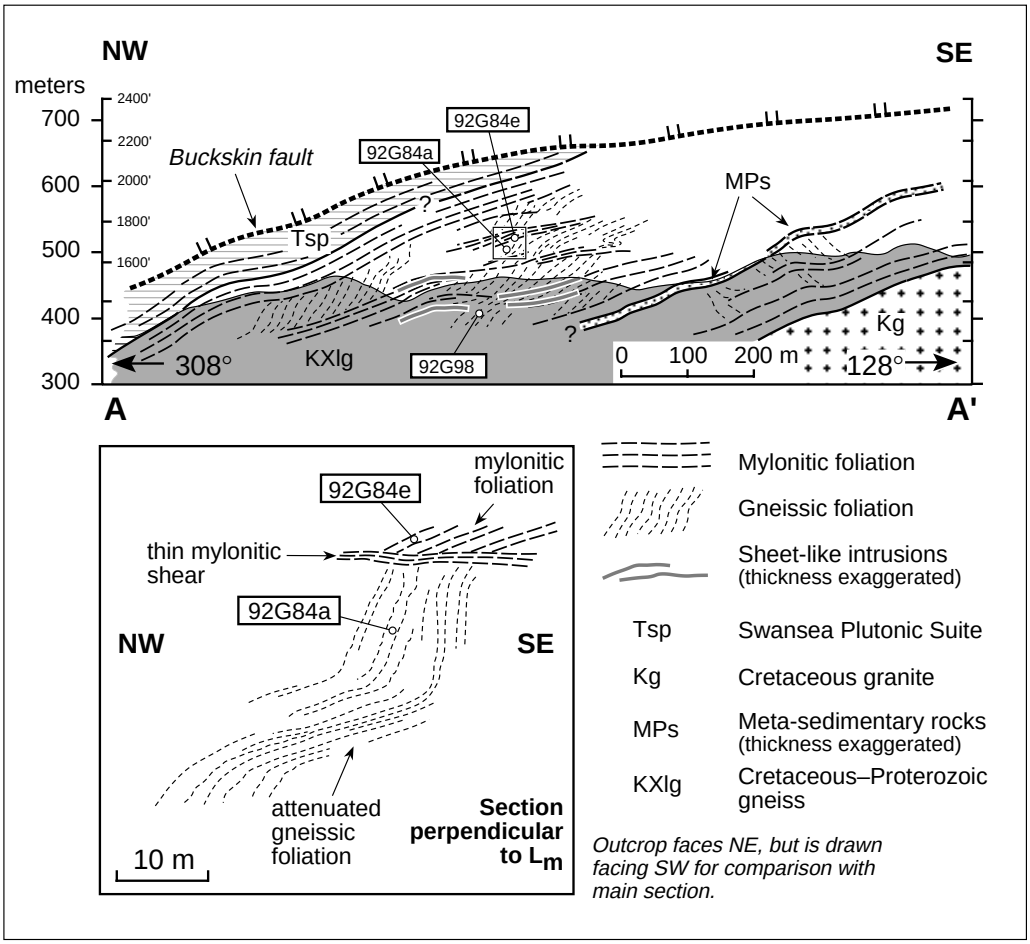

Figure 5. Cross section through the northwestern flank of the Planet Peak arch showing the relative (structural) positions of sample sites 92G84a, 92G84e, and 92G98 (see Fig. 4 for actual locations). Sample locations and the structural data used to construct the section are projected parallel to the mylonitic extension lineation (local axis of cylindricity), which plunges at 30°–35°southwest in this area. A strong mylonitic fabric is pervasively developed for as much as 100 m below the detachment fault. However, at greater depth the mylonitic fabric is generally best developed adjacent to, or along strike from, thin sheet-like synextensional intrusions, and occurs in zones from a few centimeters to >50 m thick. A predominantly steeply dipping, northeast-trending Proterozoic plus or minus Cretaceous gneissic fabric is preserved in domains as thick as 80 m thick between the mylonite zones. Inset shows structural relations at the sample site for 92G84a and 92G84e.

Conglomerate (Yarnold, 1994) indicate the Buckskin-Rawhide metamorphic core complex, and not neighboring complexes in the Harcuvar and Whipple mountains, was the source of the lower plate detritus (see Fig. 1 for relative positions of the core complexes). The origin of the lower plate detritus in the Chapin Wash Formation is less certain, although as this material is largely restricted to exposures adjacent to the exposed core of the complex (Spencer and Reynolds, 1989; Yarnold, 1994), local derivation is again considered most likely. However, predominantly southward-directed paleocurrents for the Chapin Wash Formation indicate the lower plate of the Buckskin-Rawhide core complex did not form a prominent topographic feature until just prior to the deposition of the Sandtrap Conglomerate (Yarnold, 1994).

Widespread exposure of the lower plate by 13.3 ± 2.1 Ma is indicated by a K-Ar whole-rock age (Eberly and Stanley, 1978, recalculated by Reynolds et al., 1986) for the Cobwebb Basalt, which locally underlies the Sandtrap Conglomerate. However, absolute constraints on initial exposure of the lower plate are poor. Whole-rock K-Ar ages for the stratigraphically highest volcanic unit(s?) underlying the Chapin Wash Formation vary by ~5 m.y. (21 ± 3.6 Ma: Eberly and Stanley, 1978; 16.2 ± 0.4 Ma: Shackelford, 1980; 19.2 ± 0.7 Ma: Otton, 1982; 20.2 ± 0.9 Ma and 15.8 ± 0.5 Ma: Spencer et al., 1989a). In the area north of the Buckskin-Rawhide Mountains an arkosic sequence correlative with the Chapin Wash Formation contains felsic tuff and rhyolite as old as 15.1 ± 0.1 Ma (K-Ar sanidine, Suneson and Lucchitta, 1979). Existing thermochronological data for lower plate rocks at the southwestern end of the core complex indicate the shallowest level mylonitic rocks were not exposed until after 17 Ma (e.g., Richard et al., 1990). Assuming mylonitic clasts within the Chapin Wash Formation were locally derived, 16.2 Ma appears to be the only feasible maximum age limit for surface exposure of the mylonitic core. Accordingly, initial exposure of the lower plate in the Buckskin-Rawhide Mountains probably occurred between 16.2 and 15.1 Ma, but definitely by 13.3 Ma (Fig. 3).

Previous Thermochronological Studies

Previous thermochronological studies in the Buckskin-Rawhide Mountains were primarily concerned with constraining the age of extensional deformation, rather than the cooling history of the lower plate. However the existing data reveal a consistent 1–2 m.y. difference between

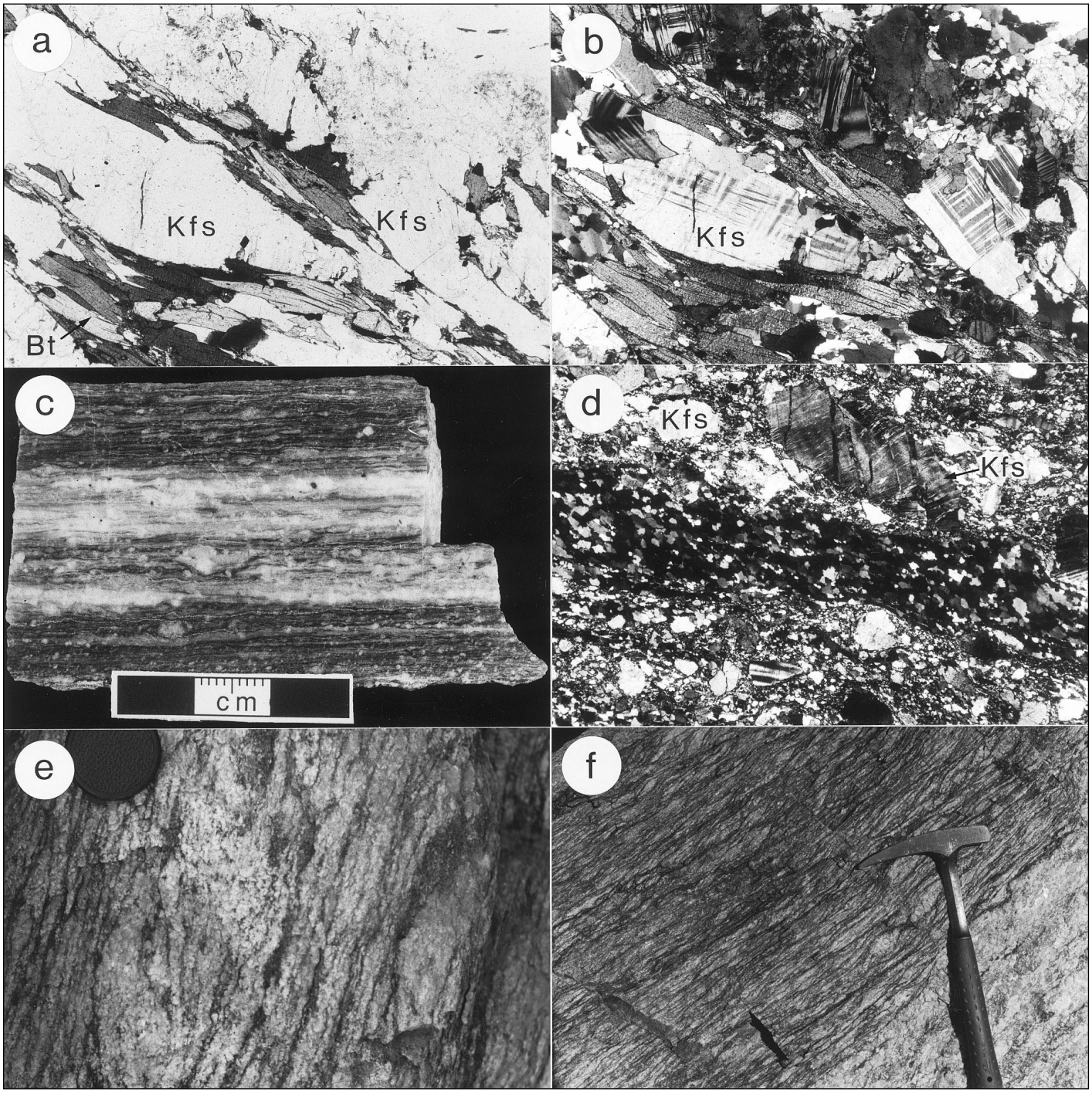

Figure 6. (a) and (b) Photomicrographs of sample 92G84a in plane- and cross-polarized light, respectively. The pre-Tertiary gneissic foliation dips from upper left to lower right. Large K-feldspar porphyroblasts (Kfs) have well-developed tartan twinning characteristic of microcline, and range from strain free to slightly kinked or fractured. Biotite (Bt) is strain free or slightly kinked and has smooth to ragged and/or irregular grain boundaries. Field of view is 3.3 × 5 mm. (c) Hand specimen of sample 92G84e showing the well-developed mylonitic fabric. (d) Photomicrograph of sample 92G84e in cross-polarized light. Quartz aggregates are extensively recrystallized and display a pronounced fabric asymmetry indicating top-to-northeast (i.e., left of photograph) shear. Original K-feldspar (Kfs) porphyroblasts are fractured and disaggregated. Field of view is 3.3 × 5 mm. (e) Well-developed gneissic layering in quartz-feldspar gneiss at the sample site for 92N48. Lens cap for scale. (f) Partially mylonitized quartz-feldspar gneiss adjacent to sample site for 92N49a. Well-developed fabric asymmetry indicates top-to-the-northeast (i.e., right of photograph) shear.

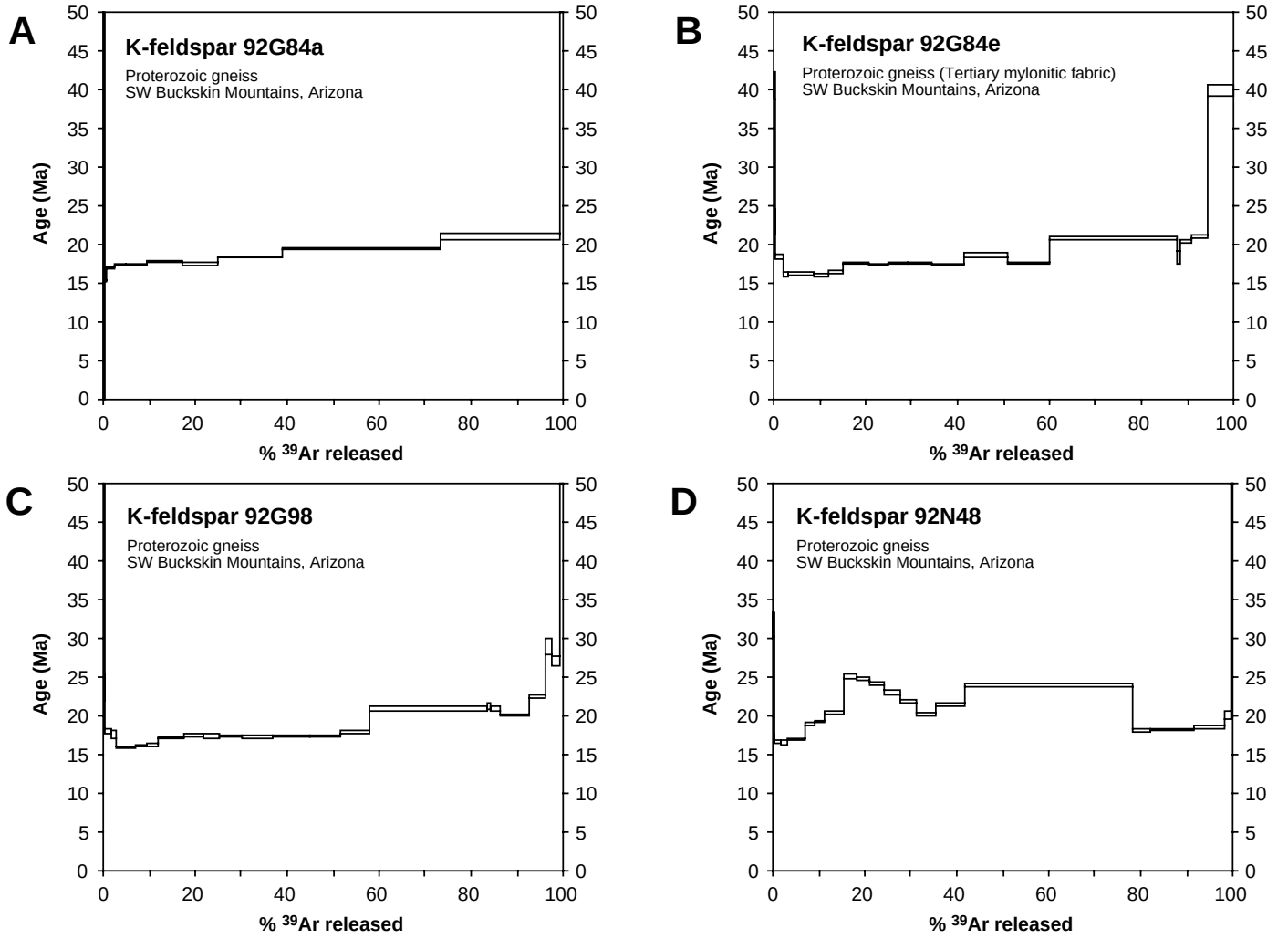

Figure 7. Apparent age spectra for K-feldspar samples from the Planet Peak area. (A) 92G84a-K: microcline from unmylonitized migmatitic gneiss. (B) 92G84e-K: microcline from strongly mylonitized migmatitic gneiss. (C) 92G98-K: microcline from unmylonitized quartz-feldspar gneiss. (D) 92N48-K: microcline from unmylonitized quartz-feldspar gneiss.

cooling ages for biotite ($^{40}Ar/^{39}Ar$ and K-Ar) and apatite (fission track) along the length of the core complex (Figs. 2 and 3), implying extremely rapid cooling during denudation of the lower plate. Closure temperatures for biotite are probably in the range 300–360 °C (for cooling rates 5–150 °C/m.y.; Harrison et al., 1985), whereas apatite fission track ages from the Buckskin-Rawhide Mountains record cooling below ~110 °C (Foster et al., 1993). These data suggest the average cooling rate at temperatures below 300 °C exceeded 100 °C/m.y. The fission track length distributions for the apatite samples also suggest cooling rates of 100–200 °C/m.y. (cf. Foster et al., 1993).

Apparent ages for biotite and apatite samples from the lower plate in the Buckskin-Rawhide Mountains both decrease toward the northeast, consistent with progressive unroofing of the lower plate in this direction (Fig. 2; Foster et al., 1993). Provided both the rate of denudation and the geothermal gradient were relatively constant during closure, the cooling ages should reflect passage through a fixed point in space (namely the closure temperature isotherm, e.g., Ketcham, 1996). Thus for each mineral, a plot of apparent age versus sample separation (measured parallel to the slip direction) yields an estimate of the slip rate on the detachment (Fig. 3; Foster et al., 1993). Due to the low uranium content and fission track density of apatite samples from the Buckskin-Rawhide Mountains, uncertainties in apparent age (s = 15%–25%) and detachment slip rate (6.6 ± 5.9 mm/yr) are correspondingly large (Fig. 3). Nonetheless, the average slip rate is similar to that inferred from the decrease in biotite age along the length of the core complex (8.7 mm/yr) and constraints on exposure of the lower plate at both ends of the complex (6.4–10.6 mm/yr, Fig. 3).

Although lower plate rocks in the Buckskin-Rawhide Mountains appear to have cooled extremely rapidly during the final stages of denudation, existing thermochronological data are not sufficient to constrain cooling rates to better than ±50 °C/m.y. The time or temperature range over which rapid cooling occurred is also poorly constrained. Although $^{40}Ar/^{39}Ar$ data for K-feldspar has potential to constrain the thermal history over the temperature range 350–150 °C (e.g., Lovera et al., 1989, 1991), the existing data from the Buckskin-Rawhide Mountains (Fig. 2; Richard et al., 1990; Fryxell, *in* Bryant,

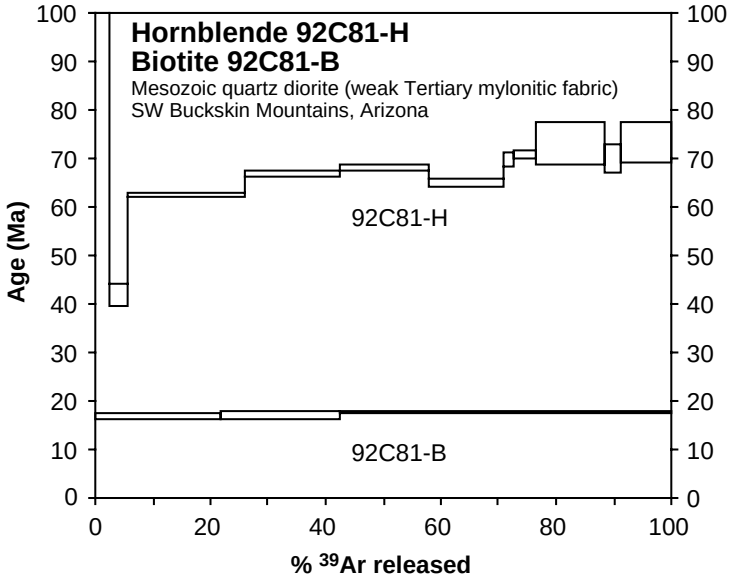

Figure 8. Apparent age spectra for hornblende and biotite from quartz-diorite sample 92C81.

1995) were not obtained in a way that is amenable to eliciting detailed thermal histories.

$^{40}Ar/^{39}Ar$ SAMPLES

$^{40}Ar/^{39}Ar$ analyses of K-feldspar, biotite, and hornblende were used to assess the cooling history of lower plate rocks at the southwestern end of the core complex (Figs. 2 and 4). The locations and apparent ages of all samples are summarized in Table 1 and detailed sample descriptions are given in Appendix 1. Four K-feldspar and three biotite separates were obtained from five samples of variably mylonitized Proterozoic gneisses on the northwestern flank of the Planet Peak arch (~3 km northwest of Planet Peak, Fig. 4). The sample sites were 150–250 m below the detachment fault (e.g., Fig. 5), in areas where the rocks were not appreciably affected by either the cataclastic deformation or propylitic (chlorite + epidote + carbonate) alteration that generally overprints lower plate rocks as much as several hundred meters below a detachment fault (e.g., Wilkins and Heidrick, 1982; Spencer and Reynolds, 1989). Samples from adjacent mylonitic and nonmylonitic rocks (Figs. 5 and 6) were chosen in order to determine whether differences in mylonitic fabric development were reflected by differences in the apparent thermal history (e.g., DeWitt et al., 1990; Lister and Baldwin, 1993). All of the samples were at least several tens of meters from the nearest of the thin (<1–5 m thick) synextensional intrusions, and >100 m below the 20–50-m-thick Swansea Plutonic Suite, which locally underlies the detachment fault on the northwestern flank of the Planet Peak arch. Accordingly, the $^{40}Ar/^{39}Ar$ data, particularly those from nonmylonitic rocks, are considered the most likely to reflect ambient temperatures during denudation of the lower plate.

Biotite and hornblende separates were obtained from a variably mylonitized quartz diorite intrusion 1 km southeast of Planet Peak (Figs. 2 and 4). Hornblende was analyzed in order to help constrain the age of the intrusion (previously interpreted to be Oligocene-Miocene: Bryant, 1995) and/or the maximum ambient temperature of lower plate rocks at the southwestern end of the core complex prior to extension. The apparent age of biotite from the quartz diorite helps constrain the lower temperature cooling history on the southeastern flank of the Planet Peak arch.

RESULTS

K-Feldspar

Age spectra for all but one K-feldspar sample are similar and record rapid cooling during Miocene denudation (Fig. 7). Samples 92G84a-

TABLE 1. $^{40}AR/^{39}AR$ SAMPLE LOCATIONS AND SUMMARY OF RESULTS

Sample	Rock type	Latitude (°N)	Longitude (°W)	Elevation (m)	Mineral	Method	Age (Ma)
92C81-H	Quartz diorite	34° 09.44′	113° 58.05′	597	Hornblende	Step heating	41.85–73.52*
92C81-B	Quartz diorite	34° 09.44′	113° 58.05′	597	Biotite	6W Ar ion laser	16.87–17.63 (17.36 ± 0.36)†
92G84a-B	Quartz-feldspar gneiss	34° 11.07′	114° 00.23′	476	Biotite	6W Ar ion laser	16.4 ± 0.5§ 23.7 ± 0.2§,#
92G84a-K	Quartz-feldspar gneiss	34° 11.07′	114° 00.23′	476	K-feldspar	Step heating	15.39–20.95*
92G84e-K	Mylonitic quartz-feldspar gneiss	34° 11.06′	114° 00.23′	486	K-feldspar	Step heating	16.08–21.1*
92G98-K	Quartz-feldspar gneiss	34° 11.11′	114° 00.19′	427	K-feldspar	Step heating	15.98–22.45*
92N48-B	Quartz-feldspar gneiss	34° 11.39′	114° 00.14′	437	Biotite	6W Ar ion laser	17.8 ± 0.2§
92N48-K	Quartz-feldspar gneiss	34° 11.39′	114° 00.14′	437	K-feldspar	Step heating	16.58–20.07*
92N49a-B	Mylonitic quartz-feldspar gneiss	34° 11.38′	114° 00.13′	439	Biotite	6W Ar ion laser	17.6 ± 0.2§

Note: Samples are stored in the Department of Earth Sciences collection, Monash University, Victoria, Australia. Errors in all ages quoted at ±1σ.

*Range in apparent age excluding steps with anomolous ages reflecting excess argon.

†Range in apparent age for 3 heating steps on single sample, total fusion age in brackets.

§Total fusion age.

#Apparent ages for two splits from the same sample.

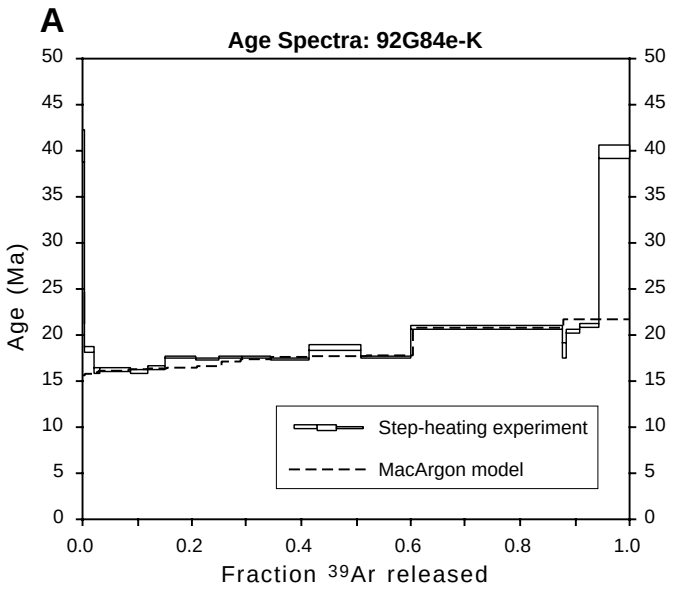

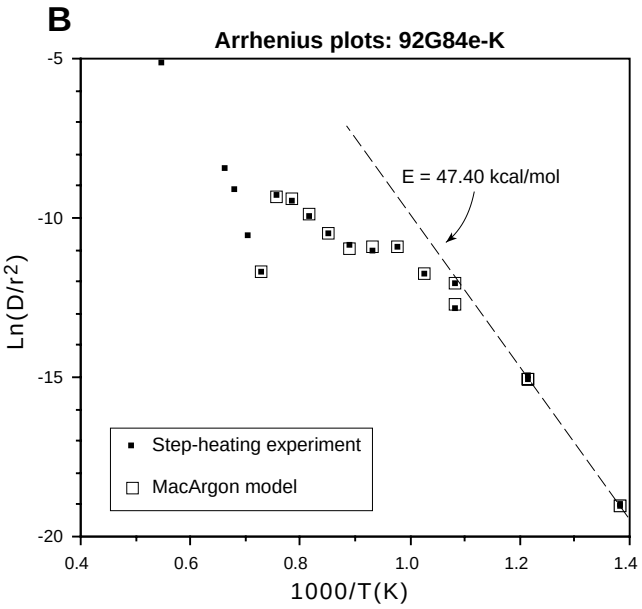

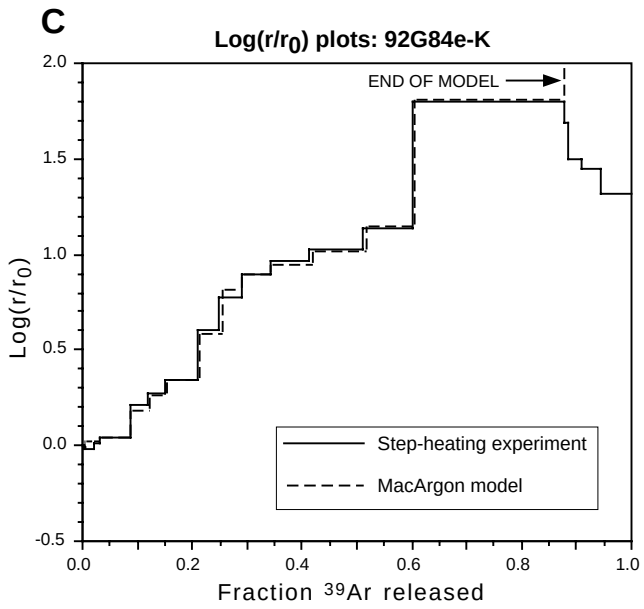

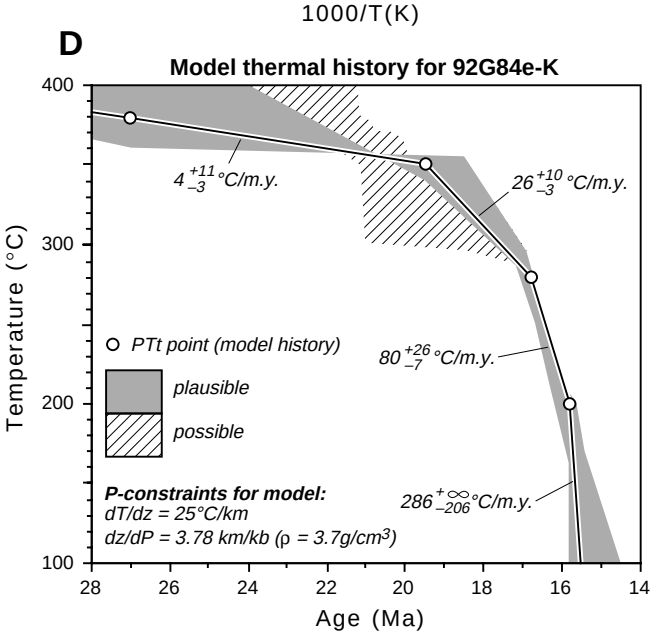

MacArgon model parameters

Activation energy = 47.40 kcal/mol
Plane sheet diffusion model

Dom.	D_0/r^2	Vol. fract.
I	1.20e+08 /s	0.053
II	6.40e+06 /s	0.152
III	3.80e+04 /s	0.395
IV	2.40e+02 /s	0.400

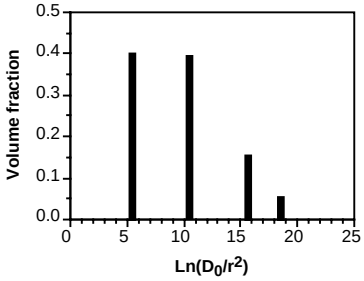

Model PT-history

P (kb)	T (°C)	t (Ma)	dT/dt (°C/m.y.)	dz/dt (mm/yr)
4.0	380	27.0	N.D.	N.D.
3.7	350	19.5	4.0	0.2
3.0	280	16.8	25.9	1.0
2.1	200	15.8	80.0	3.2
0.0	0	15.1	285.7	11.4

K, 92G84e-K, and 92G98-K all yielded relatively flat age spectra that increase from 15.5–16.5 Ma for the first 1%–15% $^{39}Ar_K$ released to about 22 Ma over the final 25%–40% $^{39}Ar_K$ (Fig. 7, A–C)[1]. Apparent ages older than 15.5 Ma and older than 22–23 Ma for the initial and final heating steps, respectively, are interpreted to reflect the presence of small amounts of excess argon (e.g., McDougall and Harrison, 1988). In samples 92G84a-K, 92G84e-K, and 92G98-K, heating steps that yielded anomalously old apparent ages accounted for <8% of the total $^{39}Ar_K$ released. Sample 92N48-K yielded a more highly disturbed age spectrum due to the release of excess argon from the larger diffusion domains over the majority of heating steps (Fig. 7D; e.g., Foster et al., 1990b). As is commonly observed for K-feldspars exhibiting excess argon in large diffusion domains (Foster et al., 1990b), apparent ages for the first 8% and last 20% of the $^{39}Ar_K$ released from sample 92N48-K are similar to those obtained for the other K-feldspar samples. This suggests that all lower plate rocks in this area were at temperatures above the upper limit for argon retention in K-feldspar during the early stages of extension and subsequently cooled through closure at about the same time.

[1]GSA Data Repository item 9820, Tables DR1–DR6, containing additional $^{40}Ar/^{39}Ar$ data including heating schedules for K-feldspar and hornblende samples, is available on request from Documents Secretary, GSA, P.O. Box 9140, Boulder, Colorado 80301. E-mail: editing@geosociety.org.

Biotite

Apparent ages for biotite from the Planet Peak area are slightly more variable than those of the K-feldspar samples (Tables 1 and DR6; see footnote 1). In particular, biotite splits from sample 92G84a-B yielded discordant bulk-fusion ages of 16.4 ± 0.5 and 23.7 ± 0.2 Ma. However, biotite from adjacent mylonitized (92N49a-B) and unmylonitized (92N48-B) Proterozoic gneisses yielded concordant bulk-fusion ages of 17.6 ± 0.2 Ma and 17.8 ± 0.2 Ma, respectively. Biotite from the quartz diorite southeast of Planet Peak (degassed in three steps) showed an increase in apparent age from 16.9 ± 0.5 Ma for the first 22% ^{39}Ar released to 17.6 ± 0.1 Ma over the last 57.6% ^{39}Ar released (Fig. 8, and Table DR6 [see footnote 1]). The equivalent total-fusion age for this sample was 17.4 ± 0.4 Ma, similar to the apparent ages for biotite samples 92N48 and 92N49a, suggesting that the exposed lower plate rocks on both flanks of the Planet Peak arch cooled through biotite closure at about the same time. Given the similarity of most biotite $^{40}Ar/^{39}Ar$ apparent ages in the Planet Peak area (including the 17.0 Ma Richard et al. [1990] sample, Fig. 2), it is likely that the 23.7 Ma total-fusion age for one split from 92G84a-B reflected the presence of excess argon, incorporated during lower greenschist facies chloritization or subsequent propylitic alteration.

Hornblende

Sample 92C81-H yielded a regularly shaped age spectrum that is relatively flat over the last 75% ^{39}Ar released. The apparent age increases from 41.9 ± 2.3 Ma (2.6%–5.7% $^{39}Ar_K$ released; Table DR1 [see footnote 1] and Fig. 8) to a maximum of 72.9 ± 4.1 Ma (total fusion age for last 24% $^{39}Ar_K$ released). This indicates that the quartz diorite is at least Late Cretaceous in age, and not part of the Swansea Plutonic Suite, as previously thought (cf. Bryant, 1995; Scott, 1995). The 66.7 Ma total fusion age for sample 92C81-H (excluding step 1) is >90% of the maximum age, suggesting that <10% of the $^{40}Ar^*$ accumulated since Late Cretaceous time was lost prior to final closure in Oligocene time.

The maximum apparent age for sample 92C81-H is concordant with a 73 ± 3 Ma U-Pb age for zircon (Wright et al., 1986) from the compositionally similar Axtel quartz diorite, exposed in the neighboring Whipple Mountains (Anderson and Rowley, 1981; Anderson and Cullers, 1990). This suggests that the intrusion may be Cretaceous in age. Although lower plate rocks exposed near Planet Peak may not have been as strongly affected by Cretaceous metamorphism as those to the northeast (where

Figure 9. MacArgon modeling of $^{40}Ar/^{39}Ar$ data for sample 92G84e-K. (A) Comparison of real and model age spectra for sample 92G84e-K. The model age spectrum is based on the four-domain model and pressure-temperature (*P-T*) history specified to the right of the figure (*t* is time). (B) Comparison of real and model Arrhenius data for 92G84e-K. The *y*-axis gives a measure of the relative diffusivity, i.e., $Ln(D/r^2)$, of the sample based on the fraction of $^{39}Ar_K$ released during each heating step (see McDougall and Harrison, 1988, for details). The activation energy of the diffusion domains in the model is determined from the slope of the straight line through the four lowest-temperature steps, i.e., two steps at both $1000/T = 1.383$ and 1.215. If the sample consisted of a single set of domains of size r_0, the *y*-intercept (i.e., $1000/T = 0$) of the regression line defines the apparent resistivity of the sample at infinite temperature. Even though r_0 has no physical significance, it is useful for quantifying variations in the apparent retentivity of the sample during the remaining heating steps (shown graphically in C). (C) Comparison of real and model $\log(r/r_0)$ plots for sample 92G84e-K. This plot reflects the variation in retentivity of the sample with respect to the proportion of $^{39}Ar_K$ released, and gives the clearest indication of how closely the four-domain diffusion model matches the observed $^{39}Ar_K$ release. $\text{Log}(r/r_0)$ is half the difference between the apparent retentivity at each heating step, i.e., $\log(D/r^2)$, and the equivalent value of $\log(D/r_0^2)$ at the same temperature (see Lovera et al. [1991] for details). Constraints on sample diffusivity as a function of temperature were only obtained for heating steps prior to incongruent melting at 1150 °C, which is reflected by the abrupt decrease in $\log(r/r_0)$ at 87.8% $^{39}Ar_K$ released. (D) *P-T-t* paths consistent with the age spectrum and four-domain diffusion model for sample 92G84e-K. The shaded area represents the range of probable thermal histories consistent with cooling below 450 °C by 30 Ma and the assumption of no reheating during the initial stages of extension. With no constraint on the maximum temperature prior to 22 Ma, the range of viable thermal histories includes the hachured area. The limits of the shaded and hachured regions represent the extremes defined by a range of trial thermal histories consistent with the age spectrum and diffusion model for sample 92G84e-K. This does not mean that any *T-t* path within these regions is necessarily consistent with the age spectra. A pressure correction was included in the thermal models by assuming that there was a constant geothermal gradient of 25 °C/km and that cooling kept pace with denudation. However, for the range in pressure (0–4 kbar) and cooling rates prior to 16 Ma (<150 °C/m.y.), removing the pressure correction decreases the calculated temperatures by no more than 15 °C, and substantially alters the form of the predicted thermal history.

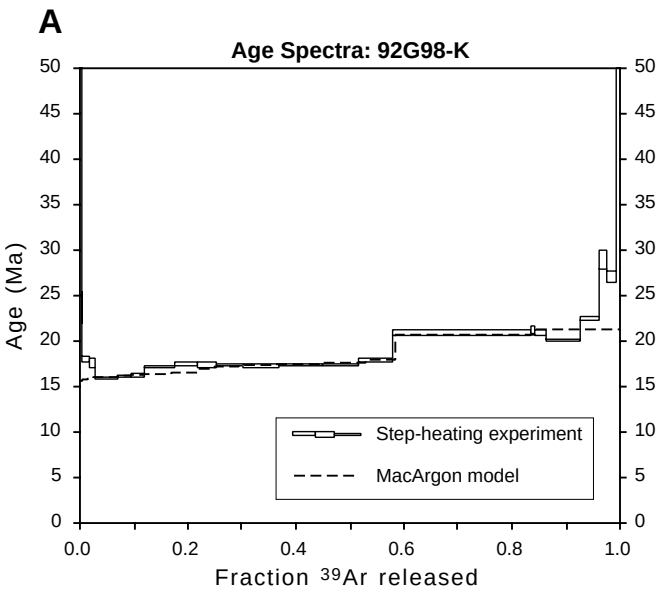

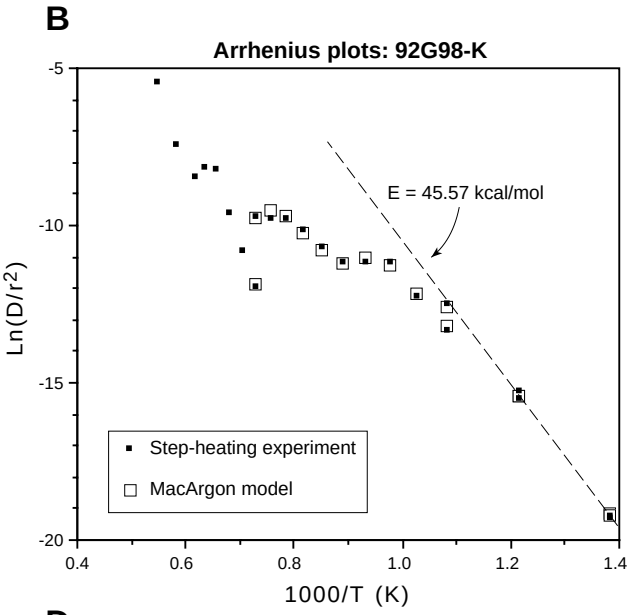

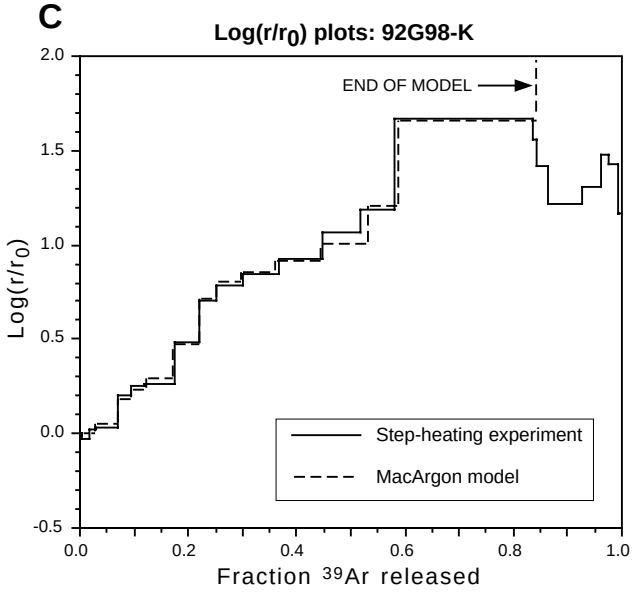

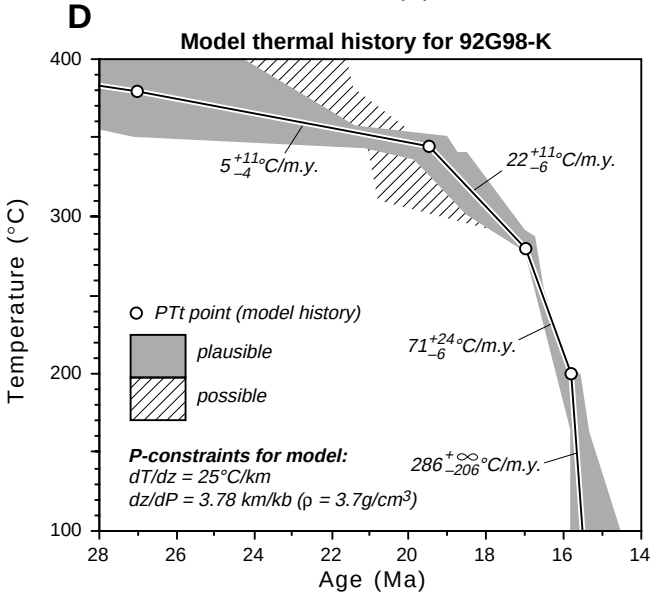

MacArgon model parameters

Activation energy = 45.57 kcal/mol
Plane sheet diffusion model

Dom.	D_0/r^2	Vol. fract.
I	5.60e+07 /s	0.035
II	2.00e+06 /s	0.140
III	1.44e+04 /s	0.365
IV	1.10e+02 /s	0.460

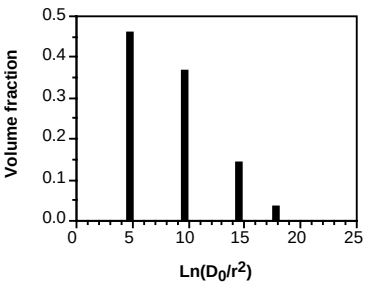

Model PT-history

P (kb)	T (°C)	t (Ma)	dT/dt (°C/m.y.)	dz/dt (mm/yr)
4.0	380	27.0	N.D.	N.D.
3.5	340	19.5	5.3	0.2
3.0	285	17.0	22.0	0.9
2.1	200	15.8	70.8	3.3
0.0	0	15.1	285.7	5.3

$^{40}Ar/^{39}Ar$ ages for hornblende in Proterozoic rocks were all reset; Fig. 2), the maximum apparent age for 92C81-H could also reflect postmetamorphic cooling. The presence of a weakly developed, steeply dipping gneissic fabric within the quartz diorite (see Appendix 1) is consistent with amphibolite facies metamorphism following emplacement of the intrusion. Accordingly, the quartz diorite near Planet Peak may be Cretaceous, Jurassic, or even Proterozoic in age.

THERMAL MODELING OF $^{40}Ar/^{39}Ar$ DATA

K-Feldspar

An apparent increase in the retentivity of samples 92G84e-K and 92G98-K with cumulative fraction ^{39}Ar released (indicated by the increase in log $[r/r_0]$ in Figs. 9C and 10C) is an intrinsic property of K-feldspar during in vacuo step heating (Lovera et al., 1989, 1991; Foster et al., 1990b; Harrison et al., 1991, 1992). This is interpreted to indicate that K-feldspars contain multiple diffusion domains that have different closure temperatures. Typically, variations in argon retentivity during step heating of single samples suggest that closure temperatures for the diffusion domains in K-feldspar range from ~170 to >350 °C (for dT/dt = 5–50 °C/m.y., pressure (P) < 4 kbar; e.g., Lovera et al., 1989; Dunlap et al., 1995). Provided argon diffusion during step-heating occurs by the same mechanism as in nature, as it appears (Lovera et al., 1991, 1993), the variation in diffusivity as a function of temperature can be combined with the age spectra to yield possible thermal histories for the sample over the temperature range represented by closure intervals for the individual diffusion domains.

For the purposes of modeling argon diffusion in K-feldspar, it is assumed that all diffusion domains in a given sample have the same activation energy (E) and frequency factor (D_0) (e.g., Lovera et al., 1991). Diffusivity of the sample as a function of temperature thus depends only on the number (n), size (r), and volume fraction (f) of the various domains. An empirical model for diffusivity of a given sample is found by determining values of the parameters n, r, and f for which the model (subjected to the same heating schedule) yields the same ^{39}Ar release pattern as the sample (Lovera et al., 1989, 1991). However, because the domain size can not be determined directly, the grouped parameter D_0/r^2 is used for the calculations. In practice, a range of domain distributions may account for the observed ^{39}Ar release. However, provided the limits of argon retentivity for the sample are reasonably well constrained by the step-heating experiment, all multidomain models that account for the ^{39}Ar release during step-heating yield essentially similar thermal histories (Lovera et al., 1991).

Tightly constraining the limits of argon retentivity of a sample is critically dependent on the heating schedule used to degas it. If the initial heating steps are too long or at too high a temperature, the smallest (least retentive) domains may be degassed in too few steps to adequately characterize their diffusivity. Alternately, if the sample melts prior to extraction of >90%–95% of the ^{39}Ar, the diffusivity of the largest domains may not be well constrained. Because the retentivity of the largest (most retentive) domains constrains the minimum temperature during initial closure of the sample, and retentivity of the smallest domains constrains the maximum temperature during final closure, uncertainty in the diffusivity of these domains means that the choice of domain distribution can affect the range of thermal histories calculated for the sample. In other words, domain distributions that produce equally good fits to the ^{39}Ar release (prior to melting) can imply very different thermal histories during both initial closure of the largest domains and final closure of the smallest domains in the sample.

Samples 92G84e-K, 92G98-K, and 92N48 were all degassed using heating schedules designed to enable characterization of the diffusivity of the samples as a function of temperature, while liberating sufficient argon in each step to facilitate accurate determination of the apparent age. Owing to the irregular form of the age spectra for sample 92N48-K (reflecting the presence of excess argon) it is of little use in assessing the thermal history. Thus only $^{40}Ar/^{39}Ar$ data for samples 92G84e-K and 92G98-K were analyzed in detail.

The correspondence between the predicted (model) and experimental ^{39}Ar release is generally improved by increasing the number of diffusion domains in the model (typically as many as eight are used). However, unless the addition of further domains expands the limits of apparent sample retentivity, increasing the number of domains from the minimum necessary to replicate the ^{39}Ar release to better than 90%–95% accuracy does not appreciably alter the calculated range of thermal histories for the sample (O. M. Lovera, 1996, personal commun.). For simplicity, we used the minimum number of domains required to obtain a good fit to the ^{39}Ar release for our samples.

Activation energies for the diffusion domains (assumed constant for each sample; e.g., Lovera et al., 1991, 1993; Harrison et al., 1992) were determined from the slope of the straight line through the first four (lowest temperature) points

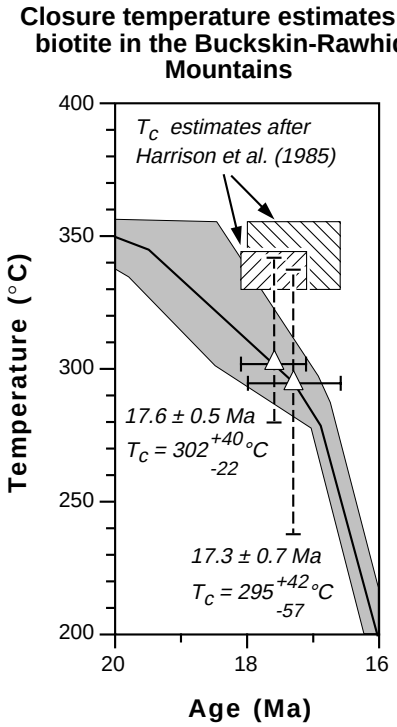

Figure 11. Estimated closure temperature (T_c) for biotite based on the average apparent ages of biotite in the Planet Peak area and the range in thermal history (shaded) consistent with $^{40}Ar/^{39}Ar$ data for K-feldspar samples 92G84e-K and 92G98-K. Hachured areas represent the calculated range in closure temperature based on published Arrhenius data for biotite (Harrison et al., 1985) at cooling rates of 20–80 °C/m.y. (inferred from K-feldspar $^{40}Ar/^{39}Ar$ data) and pressures of 2.5–3.5 kbar. See text for discussion.

Figure 10. MacArgon modeling of $^{40}Ar/^{39}Ar$ data for 92G98-K. (A) Comparison of the real and model age spectra for sample 92G98-K. The model age spectrum is based on the four-domain model and pressure-temperature (*P-T*) history specified to the right of the figure. (B) Comparison of real and model Arrhenius data for 92G98-K. See caption to Fig. 9B for further explanation. (C) Comparison of real and model log(r/r_0) plots for 92G98-K. The abrupt decrease in log(r/r_0) at 83.4% $^{39}Ar_K$ released reflects initial incongruent melting of the sample. See caption to Fig. 9C for further explanation. (D) Possible *P-T-t* (*t* = time) paths consistent with the age spectrum and four-domain diffusion model for 92G84e-K. See caption to Fig. 9D for further explanation.

on the Arrhenius plots, i.e., plots of apparent diffusivity against reciprocal temperature. Only these steps were used because the Arrhenius plots depart from linearity after the fifth step (Figs. 9B and 10B), reflecting complete degassing of the smallest domains. The activation energies determined for samples 92G84e and 92G98, 47.4 ± 0.5 and 45.6 ± 0.7 kcal/mol, respectively, are within the typical 42–48 kcal/mol range for K-feldspar (e.g., Harrison et al., 1991; T. M. Harrison, 1996, personal commun. to D. A. Foster). Almost identical activation energies were obtained using the average values determined from heating steps 1 to 3, 1 to 4, and 1 to 5. The dispersion in the individual estimates of activation energy suggests an uncertainty of ±1 kcal/mol, which is unlikely to affect the calculated thermal histories by more than ~10 °C.

We determined n, D_0/r^2, and f iteratively, using the program MacArgon 5.09 (Lister and Baldwin, 1996) to predict the percentage of $^{39}Ar_K$ released for trial domain distributions subjected to the same heating schedules as the samples. Apparent age spectra for both 92G84e and 92G98 consist of three plateau-like segments, consistent with rapid closure of three distinct domain sizes; there is a relatively small overlap between the closure intervals of successive domains. However, for both samples, a minimum of four domains was needed to obtain a reasonably good fit to the observed $^{39}Ar_K$ release (Figs. 9 and 10).

Because neither sample 92G84e-K nor 92G98-K was completely degassed prior to melting (initial melting occurred at ~88% and ~83% of the ^{39}Ar released for 92G84e and 92G98, respectively), the retentivities of the largest domains are not well constrained. However, because the minimum temperature is the only useful constraint that can ever be placed on the thermal history during the initial (i.e., highest temperature) accumulation of $^{40}Ar^*$, we determined a model domain distribution that had the least retentive large domains (maximum possible D_0/r^2) consistent with the ^{39}Ar release prior to melting. Although models that account for the gas release using more retentive domains are equally valid, these yield higher minimum estimates for the temperature during the initial closure, and thus limit the range of possible thermal histories, potentially excluding the correct one.

An initial (minimum) estimate for the retentivity of the largest domains was based on the maximum apparent retentivity, i.e., maximum $\log(r/r_0)$, of the sample prior to melting. For K-feldspar sample 92G98-K, the maximum value of $\log(r/r_0)$ was 1.67 (Fig. 10C), indicating $D_0/r^2 < 121$ for the largest domains. However, for 92G84e the maximum value of $\log(r/r_0)$ was 1.80 (Fig. 9C), indicating $D_0/r^2 < 293$ for the largest domains. Model domain distributions were determined by progressively decreasing D_0/r^2 for the largest domains (thereby increasing apparent retentivity), while adjusting their volume fraction and D_0/r^2 and f for the three smaller domains, until a satisfactory fit to the $^{39}Ar_K$ release was obtained. A trial domain distribution was considered acceptable if, for each heating step below 1150 °C, the absolute discrepancy between the predicted (model) and observed $^{39}Ar_K$ release was <0.5% and the relative error was <10%. In our four-domain models, this requirement was satisfied by heating steps representing >85% and >90% of the $^{39}Ar_K$ released below 1150 °C. The generally close match between Arrhenius and $\log(r/r_0)$ plots for the multidomain models and those based on experimental data (Figs. 9, B and C; 10, B and C) indicates that the final four domain models satisfactorily account for the $^{39}Ar_K$ release from the samples, at least over the temperature range of the step-heating experiments.

The final model parameters (i.e., n, D_0/r^2, and f) and range of thermal histories consistent with apparent age spectra for samples 92G84e-K and 92G98-K are given in Figures 9 and 10, respectively. In both samples, the closure temperatures of the smallest and largest domains differed by at least 150–165 °C (e.g., T_{cI} = 180–190 °C and T_{cIV} = 330–340 °C, at P = 2 kbar, and dT/dt = 10 °C/m.y.). Thermal histories for both samples, based on the model domain distributions, are only well constrained between 21 and 16 Ma, but both record a significant increase in cooling rate over this period. Although from a structurally deeper site in the lower plate, sample 92G98-K suggests that temperatures were consistently ~10 °C lower during denudation than those indicated by sample 92G84e-K. However when the ±1 kcal/mol uncertainty in activation energy is considered (equating to ±10 °C in the thermal history), the cooling histories recorded by these samples are indistinguishable.

Biotite

As biotite dehydrates during heating in vacuo, closure temperatures can not be directly determined from step-heating experiments (Harrison et al., 1985). However, as apparent ages for all but one of the biotite samples from the Planet Peak area are within the closure interval of the K-feldspar samples, the closure temperatures for biotite can be estimated from the calculated thermal histories for the K-feldspars. Although this does not provide additional constraints on the cooling history in the Planet Peak area, it can potentially improve thermochronological constraints elsewhere in the Buckskin-Rawhide Mountains. The biotite samples from Planet Peak area represent a variety of rock types, and most yielded apparent ages within a relatively narrow range (i.e., 17.0 and 17.8 Ma). This suggests that the closure temperature inferred for biotite in the Planet Peak area can be used to interpret K-Ar and $^{40}Ar/^{39}Ar$ ages for biotite elsewhere in the core complex, provided that cooling rates during biotite closure were fairly similar.

The average apparent age for biotite in the Planet Peak area, based on samples 92C81, 92N48, and 92N49a, is 17.6 ± 0.5 Ma, and 17.3 ± 0.7 Ma if the younger split from sample 92G84a is included. These equate to bulk closure temperatures of 302^{+38}_{-32} °C (dT/dt = 20–40 °C/m.y., P = 2.5–3.5 kbar and 295^{+45}_{-58} °C (dT/dt = 20–80 °C/m.y., P = 2.5–3.5 kbar), respectively, on the basis of the range in thermal history inferred from the K-feldspar data (Fig. 11). Closure temperatures calculated using published Arrhenius parameters for igneous biotite (composition An_{56}, Harrison et al., 1985) are >330 °C at the same cooling rates and pressures (Fig. 11). The low closure temperatures inferred for biotite samples from the Planet Peak area are unlikely to reflect additional argon loss due to deformation plus or minus recrystallization below 330 °C (cf. Goodwin and Renne, 1991). Apparent ages for biotite from adjacent mylonitized and nonmylonitized rocks are identical within error, suggesting that either grain-scale deformation did not affect argon retention in biotite, or only occurred at temperatures above the closure temperature. The lower than normal closure temperatures of the Planet Peak biotite samples may be due to as yet poorly constrained compositional effects (e.g., Grove and Harrison, 1993) or the presence of minor chlorite intergrowths reducing the effective domain size.

Hornblende

Argon loss from hornblende during in vacuo step heating is primarily a result of sample degradation rather than volume diffusion, and as a result the interpretations of apparent age spectra are controversial (J. K. W. Lee et al., 1991, 1993; Wortho, 1994). Nonetheless, hornblende apparent age spectra commonly have forms consistent with single-site volume diffusion and yield geologically reasonable age gradients or plateau ages (e.g., Harrison and McDougall, 1980; McDougall and Harrison, 1988), suggesting that argon loss during heating does broadly reflect the original distribution of $^{40}Ar^*$.

The simple form of the age spectrum for hornblende sample 92C81 and the geologically reasonable maximum age suggest the spectrum may reflect the distribution of $^{40}Ar^*$ prior to step heating, and thus provide some insight into the thermal history of the sample. The relatively flat age gradient over the last 75% $^{39}Ar_K$

released suggests that the hornblende was largely closed to argon loss in Late Cretaceous time. Final closure, represented by the minimum ages, did not occur until after 40 Ma, and possibly not until after ca. 30 Ma, although the true minimum age of the sample is obscured by excess argon in the first heating step (Table DR1 [see footnote 1] and Fig. 8). MacArgon modeling using the Arrhenius parameters for igneous hornblende (Harrison, 1981), suggests that final closure of sample 92C81-H reflects cooling below 370–410 °C (at cooling rates of 5–100 °C/m.y.). If the minimum age of sample 92C81-H is younger than 30 Ma, and thus similar to the oldest intrusions of the Swansea Plutonic Suite (e.g., Richard et al., 1990), it is possible that hornblende had closed prior to 30 Ma, but was partially degassed during the initial stages of the Oligocene–Miocene extension.

THERMAL HISTORY OF LOWER PLATE ROCKS IN THE PLANET PEAK AREA

Both the range in elevation of the Planet Peak sample sites (60 m, Table 1) and their maximum separation perpendicular to the mylonitic foliation (~100 m) are too small to be reflected by discernible differences in apparent thermal history, unless the local geothermal gradient exceeded 100 °C/km during mineral closure. However, the maximum vertical separation (and temperature difference) of the samples prior to the cessation of mylonitization is unknown. If initial closure of the K-feldspar samples occurred during mylonitization, then greater spread in the maximum ages, reflecting differences in thermal history above 300–350 °C, might be expected. Although not conclusive, the similar maximum apparent ages all of the K-feldspar samples suggests that mylonitization in the Planet Peak area may have largely ceased by 20–21 Ma.

Overall $^{40}Ar/^{39}Ar$ data for K-feldspar and biotite from the Planet Peak area provide no evidence for significant thermal heterogeneity in this part of the lower plate, at least after ca. 22 Ma. Biotite closure ages, probably reflecting cooling below ~300 °C, are the same (within error) on both flanks of the Planet Peak arch and for adjacent mylonitic and nonmylonitic rocks. $^{40}Ar/^{39}Ar$ data for K-feldspar samples 92G84e-K and 92G98-K suggest that the lower plate was at temperatures above 350–360 °C until after 21 Ma. Because the K-feldspar sample sites are located at significant but variable distances from the Swansea Plutonic Suite, these temperatures are interpreted to reflect ambient conditions rather than local thermal perturbations related to the synextensional intrusions.

Apparent ages for biotite and K-feldspar only record cooling during denudation; therefore, it is not clear whether the lower plate rocks exposed at Planet Peak remained above 360 °C until early Miocene time, or were reheated during the early stages of extension. Only the hornblende sample 92C81, which was essentially closed to argon loss prior to, or during, the early stages of extension, provides a significant constraint on the earlier thermal history. Final closure of 92C81-H, recording cooling below 370–410 °C, probably occurred after 30 Ma, suggesting that lower plate rocks in the Planet Peak area were hotter at the onset of extension than at 22 Ma. However, final closure of 92C81-H may have followed minor outgassing during emplacement of the older intrusions within the Swansea Plutonic Suite. Had lower plate rocks exposed at Planet Peak cooled below 300 °C by 30 Ma, a thermal pulse large enough to completely degas the biotite and K-feldspar samples (e.g., >2 m.y at T > 360–370 °C) would not necessarily result in appreciable argon loss from hornblende. It is clear that constraints on the thermal history of the lower plate prior to 22 Ma are poor, but although reheating during the early stages of extension is possible, it is not required to explain any of the $^{40}Ar/^{39}Ar$ data from Planet Peak.

The $^{40}Ar/^{39}Ar$ thermochronological data for the K-feldspar samples record a significant increase in cooling rate between 21 and 16 Ma. Prior to 21 Ma, infinitely fast cooling rates or rates as low as 1–2 °C/m.y. are allowed by the four domain models for samples 92G98-K and 92G84e-K. Although the true minimum age of 92C81-H is unknown with certainty, this sample provides a broad constraint for the maximum cooling rate prior to 21 Ma (assuming no reheating). The relatively minor $^{40}Ar^*$ loss from 92C81-H during early and middle Tertiary time indicates that the ambient temperature of lower plate rocks in the Planet Peak area was almost certainly <450 °C by 30 Ma. Thus the average cooling rate during the initial stages of extension was probably <15 °C/m.y.; not appreciably greater than the cooling rate during early to middle Tertiary erosional denudation in the region (e.g., Foster et al., 1990a, 1992; Knapp and Heizler, 1990).

The fastest cooling rate directly constrained by $^{40}Ar/^{39}Ar$ data for the Planet Peak K-feldspar samples is ~80 °C/m.y. at 16 Ma, but the cooling rate in this area almost certainly increased thereafter. An apatite fission-track sample from the lower plate 3.5 km northeast of Planet Peak yielded an age of 16 ± 4 Ma (Fig. 2, Foster et al., 1993), consistent with continued very rapid cooling to below 110 °C. However, because of the large uncertainty in the closure age of this sample, cooling rates could have been as low as 25 °C/m.y. after 16 Ma. Nonetheless, as Planet Peak is situated at the southwestern end of the core complex, lower plate rocks in this area were probably the first to be unroofed during top-to-the-northeast displacement on the detachment system. Age constraints for upper plate units containing lower plate detritus suggest that the lower plate first breached the surface between 13.3 and 16.2 Ma and probably before 15.1 Ma (Fig. 3). Thus, after 16 Ma the average cooling rate for lower plate rocks in the Planet Peak area was at least >80 °C/m.y. and probably >280 °C/m.y. (Figs. 9D and 10D).

COOLING-RATES ELSEWHERE IN THE BUCKSKIN-RAWHIDE MOUNTAINS

Previously published thermochronological data, although scant, provide broad constraints on the cooling history of lower plate rocks elsewhere in the core complex. In particular, when combined with estimates of closure temperature, apparent ages for muscovite, biotite ($^{40}Ar/^{39}Ar$ and K/Ar), and zircon (fission track) samples from Lincoln Ranch and the northeastern Buckskin Mountains (localities 2 and 3, respectively, Fig. 2) provide semiquantitative constraints on cooling rates during the final stages of denudation in these areas. Closure temperatures for muscovite were determined using the Arrhenius parameters given in Lister and Baldwin (1996), and those for biotite were estimated using published Arrhenius parameters (Harrison et al., 1985) and the thermochronological data from Planet Peak. Estimates of zircon closure temperature were based on data given in Foster et al. (1996) and Brandon et al. (in press). Details of cooling rate calculations are given in Appendix 3 and the results summarized in Figure 12.

Significant uncertainties in closure temperature and apparent age for most thermochronological samples from the northeastern end of the core complex mean that cooling rates are not as tightly constrained as at Planet Peak. However, for lower plate rocks in both areas, biotite closure occurred only 3–5 m.y. before exposure at the surface, indicating rapid cooling at temperatures below 350–300 °C. Lower plate rocks in the northeasternmost Buckskin Mountains (locality 3, Fig. 2) were either at, or very close to, the surface (i.e., T = 10 ± 10 °C) at 9.6 ± 0.3 Ma, following zircon closure (T_c = 258–273 °C) at 11.6 ± 0.5 Ma; this implies a cooling rate of 127^{+100}_{-42} °C/m.y. (i.e., >85 °C/m.y.) during the final stages of denudation (Fig. 12, Appendix 3). The average cooling rate of lower plate rocks in this area, following biotite closure at 12.7 ± 0.3 Ma (T_c = 377–280 °C), was at least 70 °C/m.y., i.e., 280 °C at 13.0 Ma and 20 °C at 9.3 Ma.

At both Lincoln Ranch and at the northeastern end of the core complex, the onset of moderate to rapid cooling could not have preceded biotite closure by more than 2–3 m.y. Sustained cooling rates >70 °C/m.y. prior to biotite closure would

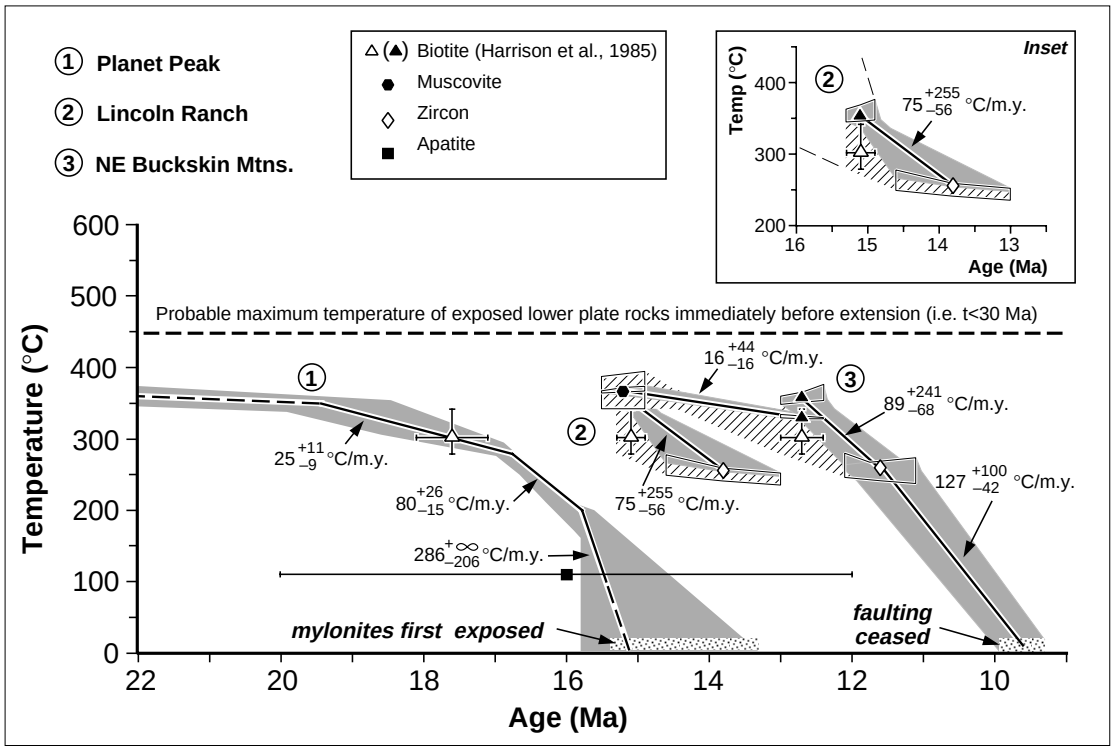

Figure 12. Miocene cooling histories for lower plate rocks at three locations along the length of the Buckskin-Rawhide Mountains (see Fig. 2 for location). At both ends of the core complex, lower-plate rocks appear to have undergone a significant increase in cooling rate below 350–300 °C. Muscovite closure temperature is estimated using Arrhenius parameters in Lister and Baldwin (1996). Biotite closure temperatures are based on both $^{40}Ar/^{39}Ar$ data from the Planet Peak area (white triangles) and Arrhenius data of Harrison et al. (1985) (black triangles). Closure-temperature estimates for zircon were determined using data in Foster et al. (1996) and Brandon et al. (in press). Boxes and error bars around mineral symbols denote uncertainty in apparent age and closure temperature. Shaded and hachured areas delineate the possible range in cooling history consistent with thermochronological data and constraints on surface exposure of the lower plate at each of the three areas. Generally lower temperatures (hachured areas) during the initial part of the recorded cooling history at localities 2 and 3 are implied by the use of the biotite closure-temperature estimate based on the thermochronological data from Planet Peak. Full details of cooling rate calculations are given in Appendix 3.

Figure 13. Hypothetical cooling histories for lower plate rocks in the Buckskin-Rawhide Mountains illustrating the effects of changes in slip rate, detachment geometry, and the development of a thermal discontinuity across the detachment. Thermochronological constraints on cooling history at (1) Planet Peak, (2) Lincoln Ranch, and (3) the northeastern Buckskin Mountains are indicated by the vertical hachures, diagonal hachures, and shading, respectively. (A) If cooling of the lower plate kept pace with denudation and the detachment was planar, the increase in cooling rate at Planet Peak could be explained by a 20-fold increase in slip rate (from 0.5 to 10 mm/yr) after 17.5 Ma. However, in order to account for the unroofing age of lower plate rocks in the northeast of the complex, a decrease in slip rate at some stage after ca. 14 Ma is required. This is in conflict with the very rapid cooling in the northeast of the complex during the final stages of denudation (note misfit between thermochronological constraints for the northeastern Buckskin Mountains and cooling curve 3). The planar detachment also requires lower plate rocks in the northeast of the complex to have been at very high temperatures (>450 °C) until a late stage during extension; this is inconsistent with the maximum metamorphic grade of the mylonites and the early Tertiary $^{40}Ar/^{39}Ar$ plateau ages for hornblende from this area. (B) The increase in the average cooling rate of lower plate rocks at temperatures below 350 °C is broadly consistent with steepening of the detachment from <5° at midcrustal levels to 24° in the upper crust, and a constant rate of horizontal extension of 6.4 mm/yr. (C) Changes in cooling rate along the length of the Buckskin-Rawhide metamorphic core complex are most consistent with both steepening of the detachment fault above the brittle-ductile transition and the development of a thermal discontinuity across the detachment fault. For a constant rate of horizontal extension of 6.4 mm/yr (equating to a slip rate of 7 mm/yr on the detachment fault), the implied time lag in the thermal response of the lower plate to denudation at Planet Peak accounts equally well for thermochronological data from the northeastern end of the core complex. Although the cooling age for zircon at Lincoln Ranch is significantly older than predicted in the model cooling history, four other zircon samples from structurally similar positions in the lower plate (see Fig. 2) yielded younger cooling ages more compatible with the model.

have required the rocks to have been at temperatures well in excess of 400 °C during the later stages of extension. In areas away from the synextensional intrusions, minerals defining the Tertiary mylonitic fabric are biotite-grade greenschist facies or below, suggesting that deformation occurred at ambient temperatures below <450 °C (Fig. 12; e.g., Spear, 1993). Higher temperature thermochronological data from the northeastern end of the core complex (hornblende, orthoclase, and muscovite) are also consistent with slow cooling at temperatures above 350 °C, suggesting that at both ends of the core complex, the lower plate underwent a marked increase in cooling rate at about 300–350 °C.

Early Tertiary K-Ar and $^{40}Ar/^{39}Ar$ plateau ages for hornblende from mylonitized Proterozoic gneisses in both the Rawhide and northeastern Buckskin Mountains (Fig. 2; Shackelford, 1980; Richard et al., 1990; Fryxell, *in* Bryant, 1995) indicate that the deepest exposed lower plate rocks had generally cooled below 500 °C well before the start of extension at ca. 27 Ma. Hornblende from a Proterozoic gneiss in the western Rawhide Mountains (Richard et al., 1990, Fig. 8a) yielded an age spectrum similar in shape to that of sample 92C81-H, consistent with rapid closure in early Tertiary time and <10%–15% $^{40}Ar^*$ loss thereafter. Final closure of the hornblende sample from the western Rawhide Mountains did not occur until after 30 Ma; however, even if it had remained open to argon loss until after 20 Ma (i.e., at $T >$ 370–410 °C), the average cooling rate for lower plate rocks in the northeast of the complex would have been <<30 °C/m.y. prior to 15 Ma. Apparent ages younger than 50 Ma for two other hornblende

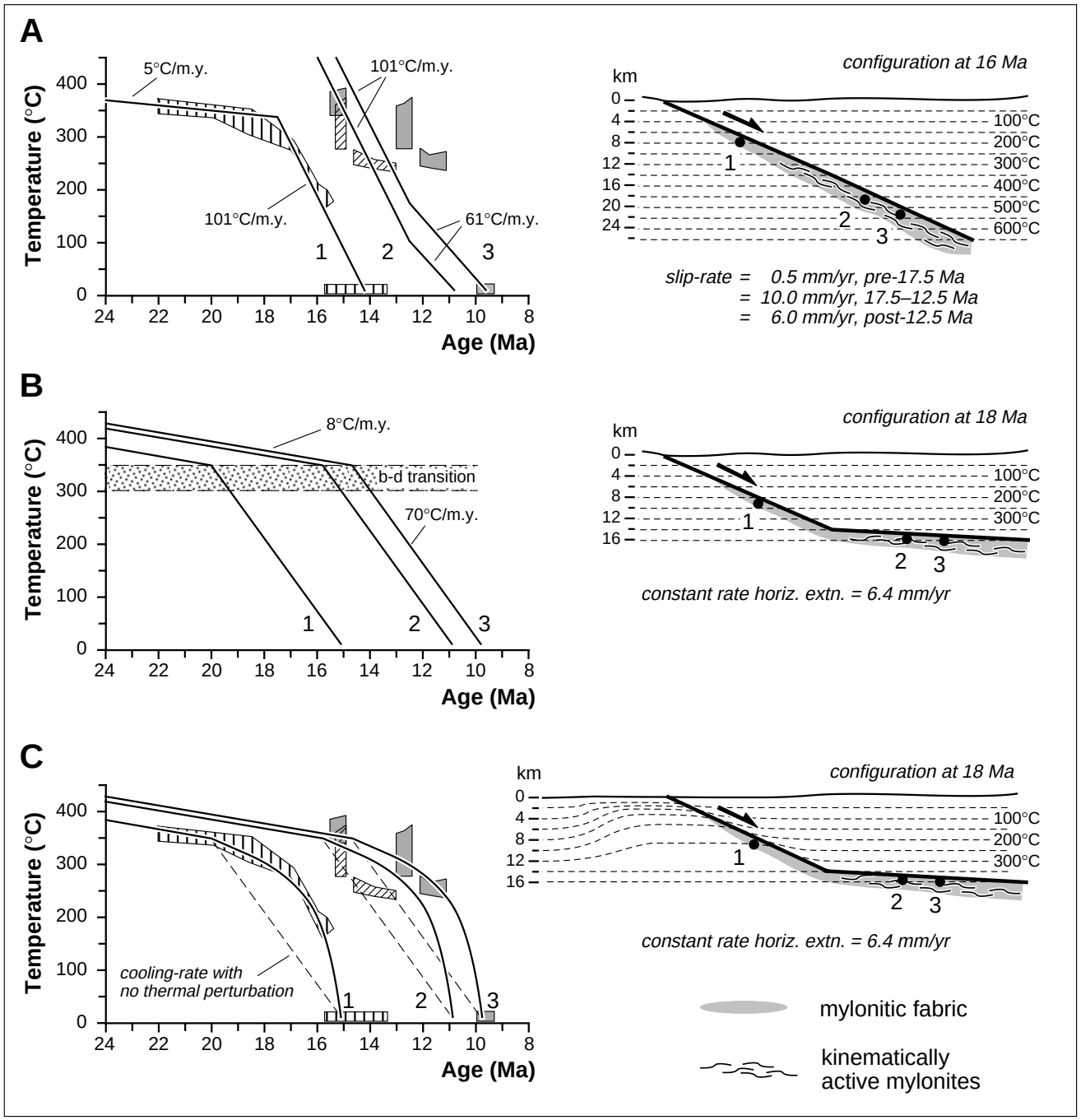

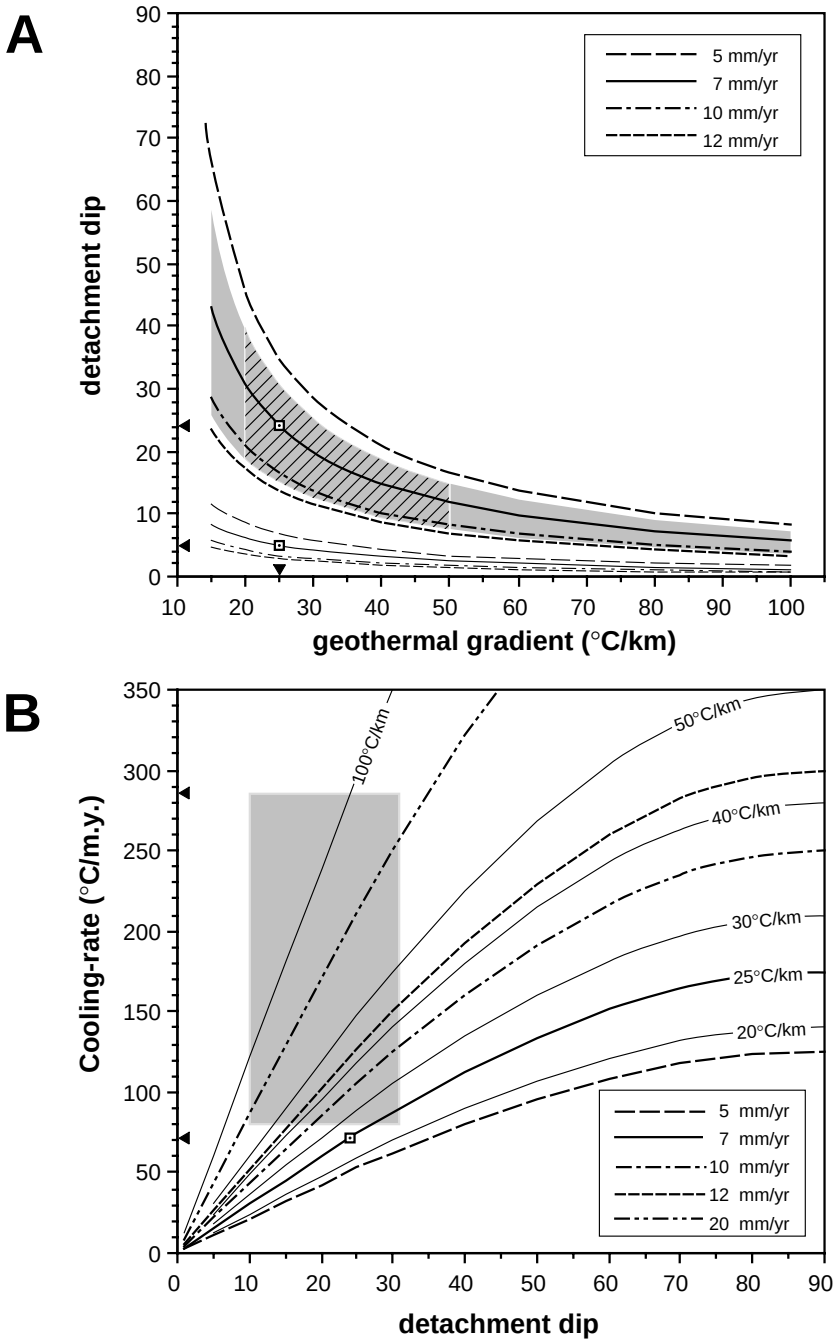

Figure 14. (A) Dip estimates for the detachment in the middle (thin lines) and upper crust (heavy lines) consistent with the average cooling rate above and below 350 °C of lower plate rocks from Planet Peak. Cooling is assumed to have kept pace with denudation along the midcrustal portion of the detachment (shear zone), i.e., temperature, T > 350 °C. Dip curves for the detachment fault were calculated assuming that lower plate rocks at Planet Peak cooled below 350 °C at 20 Ma and were exposed at the surface at 15.1 Ma. The shaded region indicates the range in dip at a slip rate of 7 mm/yr, given uncertainties in the unroofing constraints (i.e., 20 ± 1 Ma and 15.1–13.3 Ma, respectively). For slip rates of 5–12 mm/yr and geothermal gradients in the range 20–50 °C/km (hachured region), thermochronological data are consistent with the detachment fault dipping in the range 45°–10° and the shear zone dipping at <10°. Squares denote the most likely dip of the detachment fault (24°) and midcrustal shear zone (5°), given the best constraints on the slip rate and geothermal gradient. (B) Predicted cooling rate for lower plate rocks as a function of detachment dip, slip rate, and geothermal gradient. Cooling is assumed to have kept pace with denudation. Heavy lines show variation in cooling rate with dip for slip rates 5–20 mm/yr and a geothermal gradient 25 °C/km. Thin lines show same for geothermal gradients in the range 20–100 °C/km and a constant slip rate 7 mm/yr. The maximum cooling rate of lower plate rocks at Planet Peak (80–286 °C/m.y., shaded region) is well in excess of the expected 70 °C/m.y. consistent with a detachment fault dipping at 24°, a slip rate of 7 mm/yr, and geothermal gradient of 25 °C/km (denoted by square). Given the demonstrably low dip of the detachment fault, if cooling had kept pace with extension, cooling rates >280 °C/m.y. would have been possible only if slip rates exceeded 20 mm/yr or the geothermal gradient approached 100 °C/km.

samples from the Rawhide Mountains (Fig. 2) almost certainly reflect variable degrees of outgassing during emplacement of the immediately adjacent Swansea Plutonic Suite (Scott, 1995).

The $^{40}Ar/^{39}Ar$ age spectrum for an orthoclase sample from locality 3 also suggests that lower plate rocks at the northeastern end of the core complex must have cooled slowly prior to biotite closure. The apparent age increases from a minimum of younger than 11.8 Ma to a maximum of 22.7 Ma (plateau for last 40% ^{39}Ar released, Richard et al., 1990, Fig. 8b), similar to the maximum age of our microcline samples from the Planet Peak area. Although orthoclase is normally more retentive than microcline, and it is impossible to quantify the thermal history of the orthoclase sample without information constraining its diffusivity as a function of temperature, the similarity of maximum apparent ages for K-feldspar at both ends of the core complex suggests that there may not have been a large difference in the temperature of the entire exposed portion of the lower plate at 22 Ma (possibly <100 °C).

Perhaps the best constraint on cooling rates prior to biotite closure at the northeastern end of the core complex is provided by a muscovite sample from a site 5 km northwest of locality 3 (Fig. 2). Although the samples are from similar structural positions, the 15.2 ± 0.3 Ma $^{40}Ar/^{39}Ar$ plateau age for the muscovite (Fryxell, *in* Bryant, 1995) is 2.5 m.y. older than the apparent age for biotite from locality 3. Provided that both cooling ages reflect ambient temperatures in the lower plate, the average cooling rate prior to biotite closure may have been as low as 12–21 °C/m.y. (or 0–60 °C/m.y. if the lower closure estimate for biotite, based on Planet Peak thermochronological data, is used; see Appendix 3). Collectively the thermochronological data suggest that lower plate rocks at the northeastern end of the core complex had a cooling history very similar to that of the rocks exposed near Planet Peak, although the onset of rapid cooling occurred ~5 m.y. later in the northeast (Fig. 12).

DISCUSSION AND CONCLUSIONS

Controls on the Cooling Rate of Lower Plate Rocks

Although our detailed thermochronological data come from a small area at the southwestern end of the core complex, the nature of these data, coupled with the recognition of apparently similar trends in the cooling history of lower plate rocks at the northeastern end the complex, allows us to assess the main controls on the cooling rate during denudation. Factors most likely to have influenced cooling rate are: (1) the rate of denudation, (2) localized thermal perturbations associated with synextensional intrusions, and (3) variations in geothermal gradient due to either regional heating event(s) or the rapid denudation of hot midcrustal rocks.

Our analysis is in part limited by the difficulty in directly relating the cooling and denudation histories of the lower plate. This requires detailed knowledge of the geothermal gradient, slip rate, and detachment geometry throughout the development of the core complex. Although these factors are incompletely known, the slip rate (Fig. 3) and orientation of the detachment fault (Scott and Lister, 1992) are relatively well constrained after 16 Ma, when the most rapid cooling occurred. In addition, thermochronological data from two areas adjacent to the Buckskin-Rawhide Mountains (discussed below) broadly constrain the regional geothermal gradient during the early stages of extension.

The large volume of synextensional plutonic rocks emplaced in the midcrust prior to 20 Ma (Bryant, 1995) and the intermittent volcanism that continued until late Miocene time (Suneson and Lucchitta, 1983) both suggest that significant (local to regional) perturbations of the geothermal gradient may have accompanied extension in the Buckskin-Rawhide Mountains (e.g., Richard et al., 1990; Knapp and Heizler, 1990). Indeed, clear evidence for localized reheating during extension is apparent in the heterogeneity of $^{40}Ar/^{39}Ar$ apparent ages for hornblende from lower plate rocks at the northeastern end of the core complex (Fig. 2). In general, hornblende from pre-Tertiary rocks records only modest argon loss (<10%–15%) following closure in Late Cretaceous or early Tertiary time, suggesting that temperatures remained well below 450 °C throughout middle and late Tertiary time. However, samples from the immediate footwall of the Swansea Plutonic Suite, at the northeastern end of the core complex, yielded hornblende $^{40}Ar/^{39}Ar$ bulk-fusion ages in the range 49.2–31.7 Ma (Fig. 2; Scott, 1995). The youngest hornblende ages are similar to the ages of the oldest dated intrusions in the Swansea Plutonic Suite (e.g., Richard et al., 1990), suggesting that within the immediate thermal aureoles of the larger synextensional intrusions, even the most retentive K-bearing minerals were partially or completely outgassed during the early stages of extension.

In contrast, thermochronological data from Planet Peak provide no evidence for significant thermal heterogeneity at the southwestern end of the core complex, at least after ca. 21 Ma. K-feldspar samples from sites 100 and 200 m below the lower contact of the Swansea Plutonic Suite yielded indistinguishable cooling histories for the period 21–16 Ma. Similarly, in the Planet Peak area, $^{40}Ar/^{39}Ar$ cooling ages for biotite from both flanks of the lower plate arch are the same within error. This suggests that either the thermal effects of the intrusions had largely dissipated by this time, or were too weak to have significantly affected argon accumulation in K-feldspar in rocks more than 100 m from the intrusion.

In addition, there are no detectable differences in the recorded cooling histories of lower plate rocks from Planet Peak that relate to the intensity of mylonitic fabric development. MacArgon modeling of thermochronological data for the Planet Peak K-feldspar samples suggests that even the shallowest-level lower plate rocks exposed in the core complex were at "ambient" temperatures >350 °C, sufficient for ductile deformation in quartz-rich rocks, until after 20 ± 1 Ma. This is consistent with the observation that, within core complexes along the Colorado River extensional corridor, mylonites are far more widespread than intrusions of the same age (Davis et al., 1982; Spencer and Reynolds, 1991).

Volumetrically, magmatic activity in the Buckskin-Rawhide Mountains peaked prior to 20 Ma, during emplacement of the Swansea Plutonic Suite. An associated regional heating event was probably also at a maximum by or shortly after 20 Ma, and could therefore account for the high, apparently ambient, temperatures recorded immediately prior to the onset of rapid cooling at Planet Peak. However, if cooling in this area was primarily (or even strongly) influenced by the decay of such a thermal anomaly, cooling rates should have decreased with time. Even though such a thermal history was possible prior to ca. 20 Ma, it is clearly not the case thereafter, when lower plate rocks underwent a more than 10-fold increase in cooling rate with time (Figs. 9 and 10). Similarly, the average cooling rate for lower plate rocks in the northeast of the complex appears to have increased with time during extension, the most rapid cooling occurring during the 1–2 m.y. interval prior to exposure.

If the increase in cooling rate recorded by lower plate rocks was not related to either the emplacement of synextensional intrusions or a regional heating event, it must have reflected a progressive increase in the denudation rate or perturbation of the geothermal gradient due to extension. Increased denudation rates could result from either an increase in the rate of extension or steepening of the detachment system in the upper crust, whereas significant perturbation of the geothermal gradient would have occurred if cooling did not keep pace with denudation. The resultant development of a thermal discontinuity between the upper and lower plates would have led to a progressive increase in cooling rate, even if the detachment was planar and the slip rate constant.

On the basis of observations at Planet Peak

alone, it would be difficult to determine the origins of the increase in the cooling rate. However, available thermochronological data for lower plate rocks at the northeastern end of the complex are consistent with a broadly similar cooling history, relatively slow cooling at temperatures above ~350 °C, and moderate to very rapid cooling below. The onset of the abrupt increase in cooling rate appears to have occurred progressively later toward the northeast (Fig. 12), and thus can not be related to changes in slip rate alone. Changes in cooling rate related to slip rate should occur at the same time along the length of the core complex (e.g., Fig. 13A). Therefore, the abrupt increase in cooling rate recorded by lower plate rocks at Planet Peak, and inferred for lower plate rocks at the northeastern end of the core complex, must primarily reflect either the geometry of the detachment system or a systematic perturbation of the geothermal gradient as a result of extension.

Detachment Geometry

At either a constant rate of horizontal extension, or displacement on the detachment system, the denudation rate for the lower plate simply depends on the dip of the detachment. At least in the Planet Peak area, the increase in the cooling rate of the lower plate clearly commenced at temperatures corresponding to the brittle-ductile transition, and thus may have primarily reflected steepening of the detachment system in the upper crust (Fig. 13B). The slow cooling rate at temperatures above 350 °C (i.e., 1–15 °C/m.y., Figs. 9 and 10) suggests that cooling may have kept pace with denudation along the midcrustal portion (shear zone) of the detachment system. Other factors that may have influenced the cooling rate at this time, such as erosional denudation of the entire region, or a nonequilibrium geothermal gradient (related to heating during the early stages of extension), are unlikely to have been significant at 20–22 Ma and would decrease the estimated rate of tectonic denudation (and thus the inferred dip of the shear zone). Available thermochronological data suggest that any significant thermal perturbation during the initial stages of extension had probably dissipated by 22 Ma, and because the lower plate was drawn out from beneath an areally extensive network of internally drained basins (Lucchitta and Suneson, 1993), erosion is unlikely to have contributed significantly to overall denudation rates during extension.

If cooling of the lower plate kept pace with denudation along the midcrustal portion of the detachment, the geothermal gradient at this depth in the crust should have also remained largely unchanged. Accordingly, average cooling rates above and below 350 °C can be used to estimate the dip of the detachment in the upper and middle crust, respectively. Given that lower plate rocks exposed at Planet Peak cooled below 350 °C by 20 ± 1 Ma and were probably exposed at the surface by 15.1 Ma, and definitely by 13.3 Ma (Fig. 3), the average dip of the detachment fault in the upper crust was probably between 45° and 7° (Fig. 14A). This estimate is valid for geothermal gradients in the range 20–50 °C/km and for slip rates of 5–12 mm/yr. For the preferred slip rate of ~7 mm/yr (at least after 16 Ma) and a geothermal gradient of 25 °C/km (see following), the average dip of the detachment fault in the upper crust was ~24° (Figs. 13B and 14A). This is similar to estimates based on structural relations in the upper plate (e.g., Scott and Lister, 1992) and similar to the dips constrained for the upper crustal parts of detachments elsewhere in the Colorado River extensional corridor (e.g., Davis and Lister, 1988; John and Foster, 1993).

Estimating the dip of the midcrustal portion of the detachment system is more problematic, because at this depth strain was distributed across a shear zone as wide as 3 km (e.g., Davis, 1988), and the slip rate is not constrained prior to 16 Ma. Our samples were not from the base of the shear zone (e.g., Fig. 5), so their cooling histories do not necessarily reflect denudation of the lower plate as a whole; e.g., samples from the middle of a broadly symmetric shear zone should have thermal histories that reflect half the relative displacement of the hanging wall and footwall blocks. Nonetheless, K-feldspar samples 92G84e and 92G98 yielded identical cooling histories despite being collected from sites 100 m apart (measured perpendicular to the mylonitic foliation). This does not necessarily indicate that mylonitization in this area had ceased by ca. 22 Ma (i.e., during initial closure of the K-feldspars), but is consistent with relative displacement between the upper and lower plates being largely accommodated across a movement zone situated above the sample sites. If this was the case, the cooling rate of 1–15 °C/m.y. prior to ca. 20 Ma suggests that the midcrustal portion of the detachment system dipped at <1–9° for slip rates >5 mm/yr and geothermal gradients >20 °C/km (Fig. 14A). A gentle dip for the shear zone immediately below the brittle-ductile transition is consistent with thermochronological data from the northeastern end of the complex, which suggests that there may not have been a large difference in the ambient temperature of all currently exposed lower plate rocks during the early stages of extension (i.e., prior to ca. 22 Ma). However, in light of the above discussion, the dip estimate based on thermochronological data from Planet Peak should probably be regarded as a minimum for the detachment system below the brittle-ductile transition. Clayton and Okaya (1991), for example, interpreted seismic reflection data for the northeastern margin of the core complex to indicate that the detachment fault dips at 28° to a depth of 18 km, where it soles into a more gently dipping midcrustal reflective zone.

Did Cooling Keep Pace with Denudation?

In order to test whether cooling of the lower plate kept pace with denudation, and thus accurately reflects the slip rate and geometry of the detachment system (e.g., J. Lee, 1995), it is instructive to compare the maximum cooling rate of lower plate rocks with expected rates given reasonable estimates of geothermal gradient, slip rate, and dip for the detachment system. If cooling kept pace with denudation, the cooling rate is simply the product of the denudation rate and the geothermal gradient:

$$\text{Cooling-rate, } \frac{\Delta T}{\Delta t} = u \times \sin\theta \times \frac{\Delta T}{\Delta z} \quad (1)$$

where dT/dz is the geothermal gradient, u is the slip rate, and θ is the dip of the detachment. Previous estimates for the geothermal gradient in the Basin and Range Province during Tertiary time typically range between 30 and 50 °C/km (e.g., John and Foster, 1993, p. 1105). However, more recent thermochronological data from the northern Plomosa Mountains (30 km southwest of Planet Peak, Foster and Spencer, 1992) and the Mohave Mountains (~50 km northwest of Planet Peak) suggest that the geothermal gradient in west-central Arizona could have been as low as 20–25 °C/km during the early stages of extension, i.e., 22–24 Ma (Foster et al., 1994).

Thermochronological data from the Buckskin-Rawhide Mountains, coupled with constraints on surface exposure of the lower plate, suggest that maximum cooling rates exceeded 80 °C/m.y., and probably 130 °C/m.y. during the final stages of denudation at both ends of the core complex (Fig. 12). If cooling of the lower plate kept pace with denudation, and the ~25 °C/km regional geothermal gradient was maintained after 16 Ma, a cooling rate of only ~75 °C/m.y. is consistent with the probable slip rate (~7 mm/yr, Fig. 3) and dip (<25°, Scott and Lister, 1992; Scott, 1995) of the detachment fault at that time. Although there is significant uncertainty in the detachment slip rate at any stage during extension, sustained slip rates faster than 10 mm/yr are needed to explain cooling rates >130 °C/m.y., unless the detachment dipped at >30° or the geothermal gradient exceeded 35 °C/km (Fig. 14B).

Given the demonstrably low dip of the detachment fault during the latter stages of extension (Scott and Lister, 1992; Scott, 1995), the maximum cooling rate for lower plate rocks near Planet

Peak (i.e., >286 °C/m.y., assuming these rocks had breached the surface by 15.1 Ma, Fig. 12) is too high for the average slip rate on the detachment fault unless the geothermal gradient exceeded 100 °C/km (Fig. 14B). It is also significant that in the eastern Buckskin Mountains cooling rates >130 °C/m.y. occurred after 12 Ma, during the waning stages of detachment faulting, when slip rates may well have begun to decline. Thus we conclude that cooling of the lower plate could not have kept pace with denudation, at least in the upper crust above the brittle-ductile transition (i.e., $T < 300–350$ °C; Fig. 13C).

If significant perturbation of the geothermal gradient occurs at denudation rates >1 mm/yr (e.g., Ruppel et al., 1988; Stüwe et al., 1994), the maximum steady-state cooling rate for lower plate rocks in the Buckskin-Rawhide Mountains may have been as low as 25 °C/m.y. (assuming a geothermal gradient of 25 °C/km). This is approximately one-third the cooling rate required for the lower plate to have remained in thermal equilibrium with the upper plate during denudation (assuming that lower plate rocks at Planet Peak were in thermal equilibrium with their surroundings when they cooled below 350 °C at ca. 20 Ma, and were exposed at the surface by 15.1 Ma; Fig. 13B). If it is assumed that the slip rate was relatively constant over the interval 20–15 Ma, comparison between an ideal linear cooling history and the observed cooling history for lower plate rocks at Planet Peak suggests that the thermal discontinuity across the detachment fault may have exceeded 130 °C at depths of 2–6 km depth (Fig. 13C).

Ketcham (1996) used a two-dimensional finite-element model to predict the thermal histories of denuded lower plate rocks in metamorphic core complexes. The detachment geometry, slip rates, and initial geothermal gradient used in the numerical models were similar to our estimates of these parameters for the Buckskin-Rawhide metamorphic core complex (e.g., Fig. 13C). Ketcham's modeling suggests a maximum temperature discontinuity across the detachment fault in the upper crust that is somewhat less than half that we have proposed, on the basis of thermochronological data from Planet Peak. Nonetheless, both the overall form of theoretical cooling curves and temporal variations in cooling rate along the length of the core complex (Ketcham, 1996, Fig. 4) are remarkably similar to those observed or inferred for the lower plate in the Buckskin-Rawhide Mountains.

On the basis of a study of detachment-related Cu-Fe mineralization in west-central Arizona, Spencer and Welty (1986) also concluded that the lower plate must have retained much of its heat during transport to very shallow levels in the crust. Trapping temperatures for fluid inclusions indicate that the mineralizing fluids were typically between 150 and 330 °C (e.g., Spencer and Welty, 1986; Roddy et al., 1988). However, much of the mineralization is hosted by synextensional deposits that were never buried more than 1–3 km. The low geothermal gradients parallel to the detachment faults (e.g., Ruppel et al., 1988) argue against large-scale transport of deeply sourced hot fluids along the detachment fault (Spencer and Welty, 1986). Furthermore, both the mineralizing fluids and the metals appear to have been largely derived from the upper plate (Roddy et al., 1988). Since detachment-related Cu-Fe deposits are relatively widespread in west-central Arizona, but do not appear to be either spatially or temporally related to igneous intrusions, Spencer and Welty (1986) suggested that rapid uplift of hot lower plate rocks was responsible for generating the anomalously high temperatures of the mineralizing fluids at such shallow levels in the crust. It is possible, therefore, that rapid cooling of the lower plate was aided by interaction with fluids derived from upper plate reservoirs.

Can Rapid Cooling Postdate Denudation?

K-feldspar samples 92G84e and 92G98 record synchronous cooling below the lower temperature limit for ductile deformation in quartz-rich rocks. As previously noted, this does not necessarily imply that mylonitization in this area had ceased by 22–21 Ma; the vertical separation of the sampled rocks may never have been large enough to be reflected by detectable differences in thermal history. Nonetheless, our analysis of thermochronological data from Planet Peak suggests that biotite closure probably occurred at a depth of 6–9 km ($T_c \approx 300$ °C), and final closure of K-feldspar ($T_c \approx 200$ °C) may have occurred at as little as 2 km depth (Fig. 13C). It is clear that in both cases final closure postdated mylonitization at midcrustal depths.

Somewhat similar results were obtained for lower plate rocks from the Bitterroot metamorphic core complex in Idaho and Montana, where apparent ages for muscovite, biotite, and K-feldspar record rapid cooling 3–8 m.y. after the cessation of amphibolite facies mylonitization (House and Hodges, 1994). It was not clear, however, whether rapid cooling in the Bitterroot complex postdated denudation of the lower plate (exclusively correlated with mylonitization, House and Hodges, 1994) or occurred during subsequent brittle extensional faulting, i.e., continued tectonic denudation at higher crustal levels (Foster, 1995).

Our interpretation of thermochronological data from the Buckskin-Rawhide Mountains suggests that cooling of the lower plate did not keep pace with denudation, and that the onset of rapid cooling occurred relatively late in the denudation history of a particular area. However, rapid cooling clearly took place during ongoing extensional deformation. Although thermochronological data from individual core complexes should be assessed on merit, we note that the low dips generally inferred for the midcrustal portions of detachment systems (Rehrig and Reynolds, 1980; Davis and Lister, 1988; Wernicke and Axen, 1988; J. Lee, 1995) argue against the development of a significant temperature discontinuity between the upper and lower plates at the depths of mylonitization. Accordingly, we believe that rapid cooling of lower plate rocks in the Bitterroot core complex, as in the Buckskin-Rawhide Mountains, could have only occurred during continued denudation at higher crustal levels (see also Foster, 1995).

ACKNOWLEDGMENTS

This research constitutes a portion of Scott's doctoral thesis at Monash University, as well as ongoing research in the Colorado River extensional corridor by Foster. Field work was primarily funded by an Australian Research Council (ARC) Grant "Continental Extension Tectonics," to Lister, Gleadow, and Houseman. $^{40}Ar/^{39}Ar$ analyses were funded by a separate ARC grant to Gleadow, Foster, and Lister. Wayne Noble, Asaf Raza, Alan Jacka and Stan Szczepanski (La Trobe University) are thanked for assistance with $^{40}Ar/^{39}Ar$ sample preparation and analyses. Sample irradiations were undertaken at the Soreq Nuclear Research Center, Israel, and we thank the staff there for their assistance. MacArgon 5.09, used for modeling the $^{40}Ar/^{39}Ar$ data, was written by Lister. A free copy of the program can be obtained via the Internet at: http://artemis.earth.monash.edu.au/macargon. Discussions about the significance of our $^{40}Ar/^{39}Ar$ data with Oscar Lovera and Marty Grove were of considerable benefit. Constructive reviews by Stephen Richard and Bruce Bryant and editorial comments by Barbara John helped us to improve the manuscript.

APPENDIX 1. SAMPLE DESCRIPTIONS

Sample 92G84a: K-Feldspar and Biotite

Location: 34°11.07′N, 114°00.23′W. Biotite and K-feldspar mineral separates were obtained from sample 92G84a. The sample was from a >20-m-thick lens of migmatitic gneiss on the northwestern flank of the Planet Peak arch (see Fig. 4). In this area numerous similar lenses of weakly to strongly folded gneiss are cut by mylonitic shear zones and thin synextensional intrusions (see Fig. 5). Sample 92G84a preserves the steeply dipping Proterozoic gneissic fabric and was only very weakly overprinted by the Tertiary

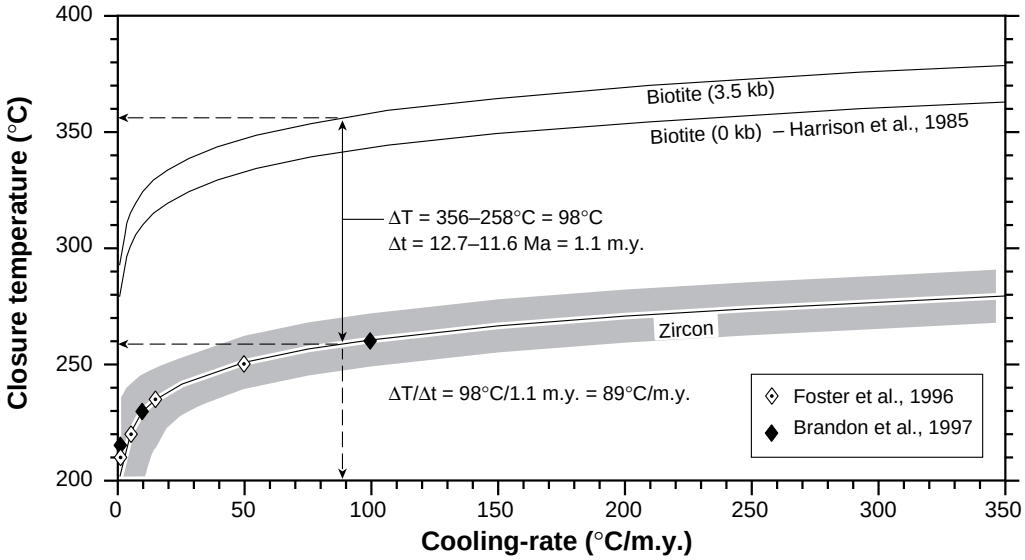

Figure A1. Calculation of cooling rates using apparent age data for biotite ($^{40}Ar/^{39}Ar$) and zircon (fission track). Closure-temperature (T_c) curves for biotite (0 and 3.5 kbar) are based on Arrhenius parameters determined by Harrison et al. (1985). The T_c curve for zircon is based on equation A4 and analytically determined closure temperatures given in Table A1. For both minerals the uncertainty in T_c at a given cooling rate is much smaller than the possible variation in T_c over a range of cooling rates. Cooling-rates consistent with apparent ages for biotite and zircon are determined by satisfying equation A4. The example shown is the average cooling rate during biotite and zircon closure in the northeastern Buckskin Mountains.

mylonitic fabric. The site is ~150 m below the detachment fault, several tens of meters from the nearest exposed synextensional intrusion and 100 m below the lower contact of the thick Tertiary intrusive suite that forms the structurally highest unit in the lower plate in this area (Figs. 4 and 5).

The gneissic fabric in 92G84a is defined by aggregates of aligned biotite and lesser muscovite as much as 3 mm wide, separated by 3–6mm-wide domains of K-feldspar, quartz, and minor plagioclase (see Fig. 6, a and b). Epidote, magnetite, apatite, and sphene are accessory minerals. Chlorite plus or minus epidote are minor retrograde phases. The quartz in 92G84a is variably recrystallized; relict grains as much as 1.75 mm in diameter. Recrystallized quartz grains are generally equant to elongate; grain sizes are 0.15–0.05 mm. A weak (incipient) mylonitic fabric is apparent in some quartz-rich domains.

The biotite laths are as long as 2 mm and typically have ragged grain boundaries, where fine-grained greenish biotite is intergrown with magnetite, quartz, muscovite, and chlorite (see Fig. 6a). The larger grains are unaltered, have strong red-brown to pale brown pleochroism, and range from strain free to slightly kinked. Smaller biotite grains generally have a faint green tinge, suggesting either partial replacement by chlorite or substitution of Mg and Si for Ti, Al, and Fe (e.g., Davis et al., 1980). The biotite contains minor (2%–5%) inclusions of magnetite(?), zircon, quartz, and apatite.

The K-feldspar in 92G84a is as much as 5 mm in diameter, and exhibits well-developed tartan-twinning characteristic of microcline (see Fig. 6b). Grains range from strain free to slightly fractured or kinked (Fig. 6b). Deformation of the feldspars is restricted to discrete kink bands, 0.05–0.025 mm thick, and minor recrystallization along grain margins. Most K-feldspar grains contain ~1% inclusions of very fine grained mica, <2.5–7.5 mm in diameter, as well as larger inclusions of plagioclase, biotite, and quartz.

Sample 92G84e: K-Feldspar

Location: 34°11.06′N, 114°00.23′W. A K-feldspar separate was obtained from sample 92G84e, a mylonitized quartz-feldspar gneiss, located ~10 m structurally above 92G84a (see Figs. 4, 5, and 6c). The gneissic domain (represented by sample 92G84a) and mylonitic domain (represented by 92G84e) are separated by a 1-m-wide late-stage mylonitic shear zone that cuts obliquely across the earlier fabrics (see Fig. 5, inset). Both generations of mylonitic fabric record top-to-the-northeast shear and are interpreted to have formed during late Oligocene or early Miocene extensional deformation. The mineralogy of 92G84e is similar to 92G84a, although chlorite and epidote are slightly more abundant in the former. Garnet and allanite are additional accessory phases in 92G84e.

Sample 92G84e exhibits considerable grain size reduction of both quartz and mica compared to sample 92G84a. Quartz grains are typically <0.1 mm (see Fig. 6d), similar to the recrystallized grains in 92G84a. Biotite is too fine grained and intergrown with retrograde phases to be separated for analysis. K-feldspars in 92G84e are more highly fractured than in the gneissic protolith (cf. Fig. 6, b and d).

Sample 92G98: K-Feldspar

Location: 34°11.11′N, 114°00.19′W. A K-feldspar separate was obtained from 92G98, a sample of moderately to weakly foliated granitic gneiss. The sample site is located 200–250 m below the detachment fault, ~100 m structurally below 92G84, and 10–20 m from the nearest synextensional intrusion or domain of Tertiary mylonitic fabric development (see Figs. 4 and 5). Sample 92G98 consists of K-feldspar, quartz, sericitized plagioclase, epidote/allanite, biotite (largely replaced by chlorite and magnetite), and minor muscovite. Mafic minerals compose <10% of the rock. K-feldspar grains as large as 1.75 mm in diameter commonly have very fine grained recrystallized margins 25 mm thick. Fractures and deformation bands, 0.125 mm thick, containing fine-grained recrystallized material are common in the larger feldspar grains. Plagioclase is extensively replaced by fine-grained sericite. K-feldspar contains a small proportion of very fine grained inclusions of mica, but is not appreciably retrogressed.

TABLE A1. ZIRCON CLOSURE TEMPERATURES

Cooling rate (°C/m.y.)	Closure temperature (°C)
Brandon et al. (in press)	
1	215
10	230
50	250
100	260
Foster et al. (1996)	
1	210
5	220 ± 10
15	235 ± 10
50	250 ± 10

Sample 92N48: K-Feldspar and Biotite

Location: 34°11.39′N, 114°00.14′W. K-feldspar and biotite separates were obtained from sample 92N48, a quartz-feldspar gneiss intermediate between 92G84a and 92G98 in composition and appearance (see Fig. 6e).

Sample 92N48 contains K-feldspar and quartz and minor biotite, plagioclase, and muscovite. Magnetite, apatite, allanite (epidote), and chlorite are accessory minerals. The sample site is located 150 m below the base of the layered Tertiary intrusive suite and ~200 m below the detachment fault (Fig. 4). Incipient recrystallization of quartz aggregates, apparent in thin section, is the only evidence for a mylonitic overprint of the steeply dipping gneissic fabric.

Most of the larger biotite grains (~2.5 mm) in 92N48 are subhedral to anhedral, and either undeformed or slightly kinked. Some have ragged edges and are typically intergrown with muscovite, chlorite, epidote, magnetite and quartz. The biotite is generally unaltered and strongly pleochroic (dark brown to reddish brown), although some grains have a slight green tinge. K-feldspar grains (microcline) in 92N48 are as much as 2.5 mm in diameter, and are slightly altered, and contain minor kink bands.

Sample 92N49a: Biotite

Location: 34°11.38′N, 114°00.13′W. A biotite separate was obtained from sample 92N49a, a mylonitized quartz-feldspar gneiss located 10–15 m southeast of sample 92N48. The intensity of the mylonitic overprint increases just to the east of 92N48 (e.g., see Fig. 6f), and is moderately well developed in 92N49a. The strong crystallographic preferred orientation and fabric asymmetry indicate that the mylonitic foliation was formed as a result of top-to-the-northeast shear. Except for the greater abundance of large (< 2 mm) grains of muscovite, the mineralogy of 92N49a is very similar to 92N48. Biotite in 92N49a is largely replaced by chlorite, although the larger (~1.5 mm) less-altered grains were separated for analysis.

Sample 92C81: Hornblende and Biotite

Location: 34°09.44′N, 113°58.05′W. Hornblende and biotite separates were obtained from 92C81, a sample from a medium-grained quartz diorite centered ~1.5 km southeast of Planet Peak (see Fig. 4). The quartz diorite forms a grossly sheet-like intrusion that has a maximum thickness of at least 350 m. The intensity of the mylonitic overprint is highly variable, but the mylonitic fabric (parallel to the upper contact) is very well developed near the top of the intrusion. A cryptic steeply northeast-dipping foliation is locally preserved in the middle to lower parts of the intrusion (including the sample site) where the mylonitic fabric is not well developed. The steeply dipping foliation is approximately parallel to, but more weakly developed than the gneissic fabric in the adjacent wall rocks.

Sample 92C81 contains plagioclase ($An_{30–33}$), hornblende, biotite, quartz, and epidote, and accessory sphene, apatite, zircon, and allanite. Retrograde epidote is abundant, and retrograde chlorite and tremolite and/or actinolite are sparse. Quartz aggregates show extensive subgrain development and undulose extinction. However, some plagioclase phenocrysts preserve original igneous textures such as delicate oscillatory zoning. Dark olive-green to blue-green hornblende is present as isolated phenocrysts or small clusters of ragged anhedral grains as much as 4 mm in length. It is commonly intergrown with (and possibly overgrown by) subhedral to euhedral biotite as much as 3 mm in length. Some hornblende contains primary rounded inclusions of plagioclase and quartz (to 0.5 mm in diameter) as well as small irregular epidote overgrowths. Hornblende forms between 20% and 30% of the sample, but is generally less abundant elsewhere in the in-

TABLE A2. ESTIMATED COOLING RATES: EASTERN BUCKSKIN MOUNTAINS

Cooling rate	Biotite apparent age (Ma)	Biotite T_c* (°C)	Zircon apparent age (Ma)	Zircon T_c † (°C)	Cooling rate (°C/m.y.)
Lincoln Ranch area: biotite (15.1 ± 0.2 Ma) and zircon (13.8 ± 0.8 Ma)					
1. Maximum	14.9	377	14.6	278	330
2. Average	15.1	354	13.8	257	75
3. Minimum	15.3	345	13.0	248	42
4. Maximum	14.9	342	14.6	273	231§
5. Average	15.1	302	13.8	248	41
6. Minimum	15.3	280	13.0	237	19
Northeastern Buckskin Mountains-I: biotite (12.7 ± 0.3 Ma) and zircon (11.6 ± 0.5 Ma)					
1. Maximum	12.4	377	12.1	278	331
2. Average	12.7	356	11.6	259	89
3. Minimum	13.0	348	11.1	251	51
4. Maximum	12.4	342	12.1	272	225§
5. Average	12.7	302	11.6	250	47
6. Minimum	13.0	280	11.1	239	21

Note: Apparent ages from Spencer et al. (1989a) and Bryant et al. (1991), see Figure 2 for locations.

*Estimates of closure temperature (T_c): 1–3 after Harrison et al. (1985); 4–6 based on thermochronological data from Planet Peak.

†Closure temperature estimates based on equation A3 (see also Fig. A1).

§Invalid, estimate of biotite closure temperature only applies for cooling rates 20–80 °C/m.y.

TABLE A3. ESTIMATED COOLING RATES: NORTHEASTERN BUCKSKIN MOUNTAINS – II

Cooling rate	Musc. apparent age (Ma)	Musc. T_c* (°C)	Biotite apparent age (Ma)	Biotite T_c † (°C)	Cooling rate (°C/m.y.)
1. Maximum	14.9	374	13.0	335	21
2. Average	15.2	369	12.7	330	16
3. Minimum	15.5	365	12.4	325	12
4. Maximum	14.9	395	13.0	280	60
5. Average	15.2	382	12.7	302	32
6. Minimum	15.5	342	12.4	342	0

Note: Estimated cooling rates based on 40Ar/39Ar apparent ages for muscovite (15.2 ± 0.3 Ma, Fryxell, *in* Bryant, 1995) and biotite (12.7 ± 0.3 Ma, Bryant et al., 1991) from the northeastern end of the core complex.

*Closure temperature (T_c) estimates based on Arrhenius data given in Lister and Baldwin (1996).

†Estimates of closure temperature: 1–3 after Harrison et al. (1985); 4–6 based on thermochronological data from Planet Peak.

TABLE A4. ESTIMATED COOLING RATES: NORTHEASTERN BUCKSKIN MOUNTAINS – III

Cooling rate	Zircon apparent age (Ma)	Zircon T_c* (°C)	Surface exposure (Ma)	Surface T (°C)	Cooling rate (°C/m.y.)
1. Maximum	11.1	273	9.9	0	227
2. Average	11.6	264	9.6	10	127
3. Minimum	12.1	258	9.3	20	85

Note: Estimated cooling-rates based on the apparent age of zircon (11.6 ± 0.5 Ma, fission track, Bryant et al., 1991) in the northeast of the core complex and surface exposure (T = 10 ± 10 °C) prior to the cessation of detachment faulting at 9.6 ± 0.3 Ma (Shackelford, 1980).

*Closure temperature estimates based on equation A3 (see also Fig. A1).

trusion. Biotite is well preserved and has strong dark brown to pale yellowish-brown pleochroism. Some grains are partially replaced or overgrown by chlorite and epidote.

APPENDIX 2. SAMPLE PREPARATION AND ANALYTICAL TECHNIQUES

Standard crushing, magnetic, and heavy liquid techniques were used to obtain mineral separates. Care was taken to concentrate the purest grains, and this was confirmed by microscopic examination of grain mounts prepared from sample splits. Separates weighing 5–10 mg were wrapped in Al foil, numbered, and placed into 1-mm-thick quartz tubes for irradiation. The sample tubes were sealed at atmospheric pressure. The sample tubes were placed inside a Cd-shielded Al canister and irradiated in two batches at the Soreq Nuclear Research Center Israel Research Reactor No. 1 (IRR-1; Heimann et al., 1992). The ratio of thermal/fast at the IRR-1 Reactor is less than 0.02 (Heimann et al., 1992).

Biotite separates from the granite gneisses were irradiated for 42 hr at 5 MW in the D-17 position of the IRR-1 reactor. The K-feldspar samples and the hornblende and biotite samples from the quartz diorite were irradiated for 49 hr in the D-17 position of the reactor. All samples were irradiated along with a biotite standard of known age (GA1550, 97.9 ± 0.9 Ma, McDougall and Roksandic, 1974). Correction factors for the production of Ar isotopes from interfering neutron-induced reactions on K and Ca were obtained by monitoring the production of these isotopes using pure K_2SO_4 and CaF_2 salts, included in the irradiation packages.

The isotopic measurements were performed at LaTrobe University using the Victorian Institute of Earth and Planetary Sciences automated VG 3600 mass spectrometer fitted to a stainless steel extraction line. Biotite samples (92G84a, 92N48, 92N49a, and 92C81) were fused in one to three heating steps using a 6W Ar ion laser. Step-heating experiments on the K-feldspar (92G84a + e, 92G98, and 92N48) and hornblende (92C81) samples were conducted using a Modification Ltd. double-vacuum resistance heated furnace. Following heating, gas liberated from the samples was expanded into the extraction line for cleaning (12 min) prior to analysis. The reactive gases were removed using a 10 L/s SAES Zr-Ti getter.

The mass discrimination and sensitivity of the mass spectrometer were determined using the measured $^{40}Ar/^{39}Ar$ ratio for aliquots of air. The system blank was periodically measured and returned $^{40}Ar/^{39}Ar$ atmospheric values. The sensitivity of the mass spectrometer is 1×10^{-3} A/torr at a 200 mA trap current. Peak heights were measured using a Daly multiplier. Isotopic ratios were determined by linearly extrapolating peak heights from six mass scans per each isotope, back to the time of gas introduction. Data reduction was performed using the program KArDate 1.9 written by Trevorrow (ANUTECH, Australian National University). Decay constants and isotopic abundances used in KArDate 1.9 are those of Steiger and Jäger (1977).

The temperature of the sample crucible in the furnace was monitored using a W-Re thermocouple in contact with the outer surface of the crucible. Samples were heated in a tantalum crucible without a liner inserted to ensure uniform and accurate temperature control. Between heating steps the temperature of the furnace was held constant at 250 °C. During heating steps the furnace temperature was set to increase from 250 °C to the required temperature at predetermined ramp rates aimed at minimizing both overshot and heating time. The precision and accuracy of the temperature measurements were ±1–2 °C and ±5 °C, respectively. For heating schedules for the hornblende and K-feldspar samples, see footnote 1.

APPENDIX 3. CALCULATION OF COOLING RATES FROM MUSCOVITE, BIOTITE, AND ZIRCON COOLING AGES

Cooling rates for lower plate rocks exposed at the northeastern end of the core complex were estimated using previously published cooling ages for muscovite, biotite (K-Ar and $^{40}Ar/^{39}Ar$), and zircon (fission track) as well as constraints on the initial surface exposure of the lower plate in this area. Determination of cooling rates requires knowledge of the variation in closure temperature, as a function of cooling rate, for each of these minerals. Muscovite closure temperatures were determined using Arrhenius parameters given in Lister and Baldwin (1996). Biotite closure temperatures were estimated using both published Arrhenius parameters (Harrison et al., 1985) and an estimate based on thermochronological data from Planet Peak. The latter is probably only valid for cooling rates in the range 20–80 °C/m.y.

Published estimates of zircon closure temperature at cooling rates of 1–100 °C/m.y. (Table A1; Foster et al., 1996; Brandon et al., in press) provide the basis for deriving an empirical relation between closure temperature and cooling rate. For fissiontrack dating, the relation between closure temperature and cooling rate is approximated by

$$B \exp \frac{E_{50}}{RT_c} = \frac{RT_c^2}{E_{50}\left(dT/dt\right)} \qquad (A1)$$

where T_c is the closure temperature, E_{50} is the activation energy for 50% track annealing, R is the gas constant, dT/dt is the cooling rate, and B is a constant (Dodson, 1979). Rearranging equation A1 yields

$$\frac{E_{50}}{RT_c} = \ln\left(\frac{R}{BE_{50}}\right) + 2\ln T_c - \ln\left(\frac{dT}{dt}\right) \qquad (A2)$$

Substituting any two closure temperature–cooling rate pairs from Table A1 into equation A2 yields two simultaneous equations that can be solved for the unknown constants E_{50}/R and $\ln(R/BE_{50})$. On the basis of the data for cooling rates ≥5 °C/m.y. in Table A1, average values for E_{50}/R and $\ln(R/BE_{50})$ are 1.88e + 4 (±6.4%) and 27.4 (±9.4%), respectively. The data for a cooling rate of 1 °C/m.y. were not used because at cooling rates <<5 °C/m.y., small uncertainties in cooling rate (±1 °C/m.y.) correspond to significant uncertainties (at least several degrees Celsius) in closure temperature. Substituting the average values for E_{50}/R and $\ln(R/BE_{50})$ into equation A2, yields:

$$\frac{1.88e + 4}{T_c} = 27.4 + 2\ln T_c - \ln\left(\frac{dT}{dt}\right) \qquad (A3)$$

which can be solved for the closure temperature of zircon at a given cooling rate (shown graphically in Fig. A1). Equation A3 yields closure temperatures within 1 °C of the analytically determined values at the same cooling rate (Fig. A1).

Given these constraints on closure temperature, cooling rates were determined iteratively, using

$$\frac{\left(T_{c_I}\right)\alpha - \left(T_{c_{II}}\right)\alpha}{\Delta t} = \alpha \qquad (A4)$$

where $(T_{cI})a$ and $(T_{cII})_a$ are closure temperatures for two different minerals at the same cooling rate, α, and dt is the difference in apparent age of the minerals. Trial values of T_{cI} and T_{cII} are substituted into Equation A4 to obtain an initial estimate of the cooling rate. T_{cI} and T_{cII} are determined at the new cooling rate and substituted back into Equation A4, yielding an improved estimate of the cooling rate. Iteration is continued until the difference in closure temperature at a particular cooling rate, divided by the difference in apparent age of the minerals, yields the same cooling rate (Fig. A1).

Estimates of the cooling rate for the lower plate in the eastern Buckskin Mountains are given in Tables A2, A3, and A4. Because a constant cooling rate during closure of successive mineral pairs is assumed, there are discrepancies in the closure-temperature estimates for biotite and zircon, depending on whether they are paired with a lower or higher temperature constraint (e.g., cf. estimates of biotite closure temperature in Tables A2 and A3). The cooling rates shown in Figure 12 are based on the full range of closure temperature estimates.

REFERENCES CITED

Anderson, J. L., and Cullers, R. L., 1990, Middle to upper crustal plutonic construction of a magmatic arc: An example from the Whipple Mountains metamorphic core complex, *in* Anderson, J. L., ed., The nature and origin of Cordilleran magmatism: Geological Society of America Memoir 174, p. 47–69.

Anderson, J. L., and Rowley, M. C., 1981, Synkinematic intrusion of two-mica and associated granitoids, Whipple Mountains, California: Canadian Mineralogist, v. 19, p. 83–101.

Baldwin, S. L., Lister, G. S., Hill, E. J., Foster, D. A., and McDougall, I., 1993, Thermochronologic constraints on the tectonic evolution of active metamorphic core complexes, D'Entrecasteaux Islands, Papua New Guinea: Tectonics, v. 12, p. 611–628.

Bennett, V. C., and DePaolo, D. J., 1987, Proterozoic crustal history of the western United states as determined by neodymium isotope mapping: Geological Society of America Bulletin, v. 99, p. 674–685.

Brandon, M. T., Roden-Tice, M. K., and Garver, J. I., 1998, Late Cenozoic exhumation of the Cascadia accretionary wedge in the Olympic mountains, northwest Washington State: Geological Society of America Bulletin (in press).

Bryant, B., 1995, Geologic map, cross sections, isotopic dates, and mineral deposits of the Alamo Lake 30′ × 60′ quadrangle, west-central Arizona: U.S. Geological Survey Miscellaneous Investigations Series, Map I-2489, scale 1:100 000, 3 sheets.

Bryant, B., and Wooden, J. L., 1989, Lower-plate rocks of the Buckskin Mountains, Arizona: A progress report, *in* Spencer, J. E., and Reynolds, S. J., eds., Geology and mineral resources of the Buckskin and Rawhide Mountains, west-central Arizona: Arizona Geological Survey Bulletin, v. 198, p. 47–50.

Bryant, B., Naeser, C. W., and Fryxell, J. E., 1991, Implications of low temperature cooling on a transect across the Colorado Plateau–Basin and Range boundary: Journal of Geophysical Research, v. 96, p. 12375–12388.

Bryant, B., Wooden, J. L., and Nealey, L. D., 1993, The Swansea Plutonic Suite: Synextensional magmatism in the Buckskin and Rawhide mountains, west-central Arizona: Geological Society of America Abstracts with Programs, v. 25, no. 5, p. 15.

Bryant, B., Wooden, J. L., Gehrels, G. E., and Spencer, J. E., 1996, Plutonic and metamorphic history, northern part of the Harcuvar Metamorphic core complex, Buckskin and Eastern Harcuvar Mountains, west-central Arizona: Geological Society of America Abstracts with Programs, v. 28, no. 5, p. 51.

Clayton, R. W., and Okaya, D. A., 1991, Subsurface geometry

of the Buckskin-Bullard detachment fault system beneath the Basin and Range: Colorado Plateau Transition zone, imaged by CALCRUST seismic reflection profiles in west-central Arizona: Geological Society of America Abstracts with Programs, v. 23, no. 5, p. 132.

Davis, G. A., 1988, Rapid upward transport of midcrustal mylonitic gneisses in the footwall of a Miocene detachment fault, Whipple Mountains, southeastern California: Geologische Rundschau, v. 77, p. 191–209.

Davis, G. A., and Lister, G. S., 1988, Detachment faulting in continental extension: Perspectives from the southwestern U.S. Cordillera, *in* Clark, S. P., Jr., Burchfiel, B. C., and Suppe, J., eds., Processes in continental lithospheric deformation: Geological Society of America Special Paper 218, p. 133–159.

Davis, G. A., Anderson, J. L., Frost, E. G., and Shackelford, T. J., 1980, Regional Miocene detachment faulting and early Tertiary mylonitization, Whipple-Buckskin-Rawhide Mountains terrane, southeastern California and western Arizona, in Crittenden, M. D. Jr., Coney, P. J., and Davis, G. H., eds., Cordilleran metamorphic core complexes: Geological Society of America Memoir 153, p. 79–130.

Davis, G. A., Anderson, J. L., Martin, D. L., Krummenacher, D., Frost, E. G., and Armstrong, R. L., 1982, Geologic and geochronologic relations in the lower plate of the Whipple detachment fault, Whipple Mountains, southeastern California: A progress report, *in* Frost, E. G., and Martin, D. L., eds., Mesozoic-Cenozoic tectonic evolution of the Colorado River region, California, Arizona, and Nevada: San Diego, California, Cordilleran Publishers, p. 408–432.

DeWitt, E., Sutter, J. F., and Reynolds, S. J., 1990, Mylonites aren't so hot—The cold facts: Geological Society of America Abstracts with Programs, v. 22, no. 3, p. 18.

Dodson, D. H., 1979, Theory of cooling ages, *in* Jäger, E., and Hunziker, J. C., eds., Lectures in isotope geology: Berlin, Heidelberg, Springer-Verlag, p. 194–202.

Dunlap, W. J., Teyssier, C., McDougall, I., and Baldwin, S. L., 1995, Thermal and structural evolution of the intracratonic Arltunga Nappe Complex, central Australia: Tectonics, v. 14, p. 1182–1204.

Eberly, L. D., and Stanley, T. B., 1978, Cenozoic stratigraphy and geological history of southwestern Arizona: Geological Society of America Bulletin, v. 89, p. 921–940.

Faulds, J. E., Geissman, J. W., and Mawer, C. K., 1990, Structural development of a major extensional accommodation zone in the Basin and Range province, northwestern Arizona and southern Nevada; implications for kinematic models of continental extension, *in* Wernicke, B. P., ed., Basin and range extensional tectonics near the latitude of Las Vegas, Nevada: Geological Society of America Memoir 176, p. 37–76.

Faulds, J. E., Geissman, J. W., and Shafiqullah, M., 1992, Implications of paleomagnetic data on Miocene extension near a major accommodation zone in the Basin and Range province, northwestern Arizona and southern Nevada: Tectonics, v. 11, p. 204–228.

Foster, D. A., 1995, Limits on the tectonic significance of rapid cooling events in extensional settings: Insights from the Bitterroot metamorphic core complex, Idaho-Montana: Comment: Geology, v. 23, p. 1051–1052.

Foster, D. A., and Spencer, J. E., 1992, Apatite and zircon fission-track dates from the northern Plomosa Mountains, La Paz County, west central Arizona: Arizona Geological Survey Open-File Report 92–9, 11 p.

Foster, D. A., Harrison, M. T., Miller, C. F., and Howard, K. A., 1990a, The $^{40}Ar/^{39}Ar$ thermochronology of the eastern Mojave Desert, California and adjacent western Arizona with implications for the evolution of metamorphic core complexes: Journal of Geophysical Research, v. 95, p. 20005–20024.

Foster, D. A., Harrison, T. M., Copeland, P., and Heizler, M. T., 1990b, Effects of excess argon within large diffusion domains on K-feldspar age spectra: Geochimica et Cosmochimica Acta, v. 54, p. 1699–1708.

Foster, D. A., Miller, C. F., Harrison, T. M., and Hoisch, T. D., 1992, $^{40}Ar/^{39}Ar$ thermochronology and thermobarometry of metamorphism, plutonism, and tectonic denudation in the Old Woman Mountains area, California: Geological Society of America Bulletin, v. 104, p. 176–191.

Foster, D. A., Gleadow, A. J. W., Reynolds, S. J., and Fitzgerald, P. G., 1993, Denudation of metamorphic core complexes and the restoration of the Transition zone, west central Arizona: Constraints from apatite fission track thermochronology: Journal of Geophysical Research, v. 98, p. 2167–2185.

Foster, D. A., Howard, K. A., and John, B. E., 1994, Thermochronological constraints on the development of metamorphic core complexes in the lower Colorado River area: U.S. Geological Survey Circular 1107, 103 p.

Foster, D. A., Kohn, B. P., and Gleadow, A. J. W., 1996, Sphene and zircon fission track closure temperatures revisited: Empirical calibrations from $^{40}Ar/^{39}Ar$ diffusion studies of K-feldspar and biotite, *in* Proceedings, International Workshop on Fission Track Dating: University of Ghent, 26–30 August 1996, p. 37.

Goodwin, L. B., and Renne, P. R., 1991, Effects of progressive mylonitization on Ar retention in biotites from the Santa Rosa mylonite zone, California, and thermochronological implications: Contributions to Mineralogy and Petrology, v. 108, p. 283–297.

Grove, M., and Harrison, T. M., 1993, Compositional controls governing argon loss in biotite [abs.]: Eos (Transactions, American Geophysical Union), v. 74, p. 339.

Harrison, T. M., 1981, Diffusion of $^{40}Ar/^{39}Ar$ in hornblende: Contributions to Mineralogy and Petrology, v. 78, p. 324–331.

Harrison, T. M., and McDougall, I., 1980, Investigations of an intrusive contact, northwest Nelson, New Zealand–II. Diffusion of radiogenic and excess ^{40}Ar in hornblende revealed by $^{40}Ar/^{39}Ar$ age spectrum analysis: Geochimica et Cosmochimica Acta, v. 44, p. 2005–2020.

Harrison, T. M., Duncan, I., and McDougall, I., 1985, Diffusion of ^{40}Ar in biotite: Temperature pressure and compositional effects: Geochimica et Cosmochimica Acta, v. 49, p. 2461–2468.

Harrison, T. M., Lovera, O. M., and Heizler, M. T., 1991, $^{40}Ar/^{39}Ar$ results for diffusion domains with differing activation energy: Geochimica et Cosmochimica Acta, v. 55, p. 1435–1448.

Harrison, T. M., Chen, W., Leloup, P. H., Ryerson, F. J., and Tapponnier, P., 1992, Termination of left-lateral motion along the Red River–Ailao Shan fault zone, Yunnan (PRC), and its influence on Indo-Asian tectonics: Journal of Geophysical Research, v. 97, p. 7159–7182.

Heimann, A., Steinitz, G., and Zafrir, H., 1992, Irradiation of samples for $^{40}Ar/^{39}Ar$ dating using the Soreq Nuclear Research Center IRR-1 Reactor, Israel: Nuclear Geophysics, v. 6, p. 273–286.

House, M. A., and Hodges, K. V., 1994, Limits on the tectonic significance of rapid cooling events in extensional settings: Insights from the Bitterroot metamorphic core complex, Idaho-Montana: Geology, v. 22, p. 1007–1010.

Howard, K. A., and John, B. E., 1987, Crustal extension along a rooted system of imbricate low-angle faults: Colorado River extensional corridor, California and Arizona, *in* Coward, M. P., Dewey, J. F., and Hancock, P. L., eds., Continental extension tectonics: Geological Society [London] Special Publication 28, p. 299–311.

John, B. E., 1987, Geometry and evolution of a midcrustal extensional fault system, Chemehuevi Mountains, southeastern California, *in* Coward, M. P., Dewey, J. F., and Hancock, P. L., eds., Continental extension tectonics: Geological Society [London] Special Publication 28, p. 313–335.

John, B. E., and Foster, D. A., 1993, Structural and thermal constraints on the initiation angle of detachment faulting in the southern Basin and Range: The Chemehuevi Mountains case study: Geological Society of America Bulletin, v. 105, p. 1091–1108.

Ketcham, R. A., 1996, Thermal models of core-complex evolution in Arizona and New Guinea: Implications for ancient cooling paths and present heat flow: Tectonics, v. 15, p. 933–951.

Knapp, J. H., and Heizler, M. T., 1990, Thermal history of crystalline nappes of the Maria fold and thrust belt, west central Arizona: Journal of Geophysical Research, v. 95, p. 20049–20073.

Lee, J., 1995, Rapid uplift and rotation of mylonitic rocks from beneath a detachment fault: Insights from potassium feldspar $^{40}Ar/^{39}Ar$ thermochronology, northern Snake Range, Nevada: Tectonics, v. 14, p. 54–77.

Lee, J. K. W., 1993, The argon release mechanisms of hornblende in vacuo: Chemical Geology, v. 106, p. 133–170.

Lee, J. K. W., Onstott, T. C., Cashman, K. V., Cumbest, R. J., and Johnson, D., 1991, Incremental heating of hornblende in vacuo: Implications for $^{40}Ar/^{39}Ar$ geochronology and the interpretation of thermal histories: Geology, v. 19, p. 872–875.

Lister, G. S., and Baldwin, S. L., 1993, Plutonism and the origin of metamorphic core complexes: Geology, v. 21, p. 607–610.

Lister, G. S., and Baldwin, S. L., 1996, Modelling the effect of arbitrary *P-T-t* histories on argon diffusion in minerals using the MacArgon program for the Apple Macintosh: Tectonophysics, v. 253, p. 83–109.

Livaccari, R. F., Geissman, J. W., and Reynolds, S. J., 1993, Palaeomagnetic evidence for large-magnitude, low-angle normal faulting in a metamorphic core complex: Nature, v. 361, p. 56–59.

Lovera, O. M., Richter, F. M., and Harrison, T. M., 1989, The $^{40}Ar/^{39}Ar$ thermochronometry for slowly cooled samples having a distribution of diffusion domain sizes: Journal of Geophysical Research, v. 94, p. 17917–17935.

Lovera, O. M., Richter, F. M., and Harrison, T. M., 1991, Diffusion domains determined by ^{39}Ar released during step heating: Journal of Geophysical Research, v. 96, p. 2057–2069.

Lovera, O. M., Heizler, M. T., and Harrison, T. M., 1993, Argon diffusion domains in K-feldspar II: Kinetic properties of MH-10: Contributions to Mineralogy and Petrology, v. 113, p. 381–393.

Lucchitta, I., and Suneson, N. H., 1993, Dips and extension: Geological Society of America Bulletin, v. 105, p. 1346–1356.

Lucchitta, I., and Suneson, N. H., 1994, Stratigraphic section of the Castaneda Hills–Signal area, Arizona, *in* Sherrod, D. R., and Nielson, J. E., eds., Tertiary stratigraphy of highly extended terranes, California, Arizona and Nevada: U.S. Geological Survey Bulletin 2053, p. 139–144.

Lucchitta, I., and Suneson, N. H., 1996, Timing and character of deformation along the margin of a metamorphic core complex, west-central Arizona, *in* Beratan, K. K., ed., Reconstructing the history of Basin and Range extension using sedimentology and stratigraphy: Geological Society of America Special Paper 303, p. 147–170.

Marshak, S., and Vander Meulen, M., 1989, Geology of the Battleship Peak area, southern Buckskin Mountains, Arizona: Structural style below the Buckskin detachment fault, *in* Spencer, J. E., and Reynolds, S. J., eds., Geology and mineral Resources of the Buckskin and Rawhide Mountains, west-central Arizona: Arizona Geological Survey Bulletin, v. 198, p. 51–66.

McDougall, I., and Harrison, T. M., 1988, Geochronology and thermochronology by the $^{40}Ar/^{39}Ar$ method: London, Oxford University Press, 212 p.

McDougall, I., and Roksandic, Z., 1974, Total fusion $^{40}Ar/^{39}Ar$ ages using the HIFAR reactor: Geological Society of Australia Journal, v. 21, p. 81–89.

Nielson, J. E., and Beratan, K. K., 1995, Stratigraphic and structural synthesis of a Miocene extensional terrane, southeast California and west-central Arizona: Geological Society of America Bulletin, v. 107, p. 241–252.

Otton, J. K., 1982, Tertiary extensional tectonics and associated volcanism in west-central Arizona, *in* Frost, E. G., and Martin, D. L., eds., Mesozoic-Cenozoic tectonic evolution of the Colorado River region, California, Arizona, and Nevada: San Diego, California, Cordilleran Publishers, p. 143–157.

Rehrig, W. A., and Reynolds, S. J., 1980, Geologic and geochronological reconnaissance of a northwest-trending zone of metamorphic core complexes in southern and western Arizona, *in* Crittenden, M. D., Jr., Coney, P. J., and Davis, G. H., eds., Cordilleran metamorphic core complexes: Geological Society of America Memoir 153, p. 131–158.

Reynolds, S. J., Florence, F. P., Welty, J. W., Roddy, M. S., Currier, D. A., Anderson, A. V., and Keith, S. B., 1986, Compilation of radiometric arc determinations in Arizona: Arizona Bureau of Geology and Mineral Technology Bulletin 197, 258 p.

Reynolds, S. J., Richard, S. M., Haxel, G. B., Tosdal, R. M., and Laubach, S. E., 1988, Geologic setting of Mesozoic and Cenozoic metamorphism in Arizona, *in* Ernst, W. G., ed., Metamorphism and crustal evolution of the United States (Rubey Volume VII): Englewood-Cliffs, New Jersey, Prentice-Hall, p. 467–501.

Richard, S. M., Fryxell, J. E., and Sutter, J. F., 1990, Tertiary structure and thermal history of the Harquahala and Buckskin Mountains, west central Arizona: Implications for denudation by a major detachment fault system: Journal of Geophysical Research, v. 95, p. 19973–19987.

Roddy, M. S., Reynolds, S. J., Smith, B. M., and Ruiz, J., 1988, K-metasomatism and detachment-related mineralization, Harcuvar Mountains, Arizona: Geological Society of America Bulletin, v. 100, p. 1627–1639.

Ruppel, C. L., Royden, L. H., and Hodges, K. V., 1988, Thermal modeling of extensional tectonics: Application to pressure-temperature-time histories of metamorphic rocks: Tectonics, v. 7, p. 947–958.

Scott, R. J., 1995, The geological development of the Buckskin-Rawhide metamorphic core complex, west-central Arizona [Ph.D. dissert.]: Clayton, Victoria, Canada, Monash University, 472 p.

Scott, R. J., and Lister, G. S., 1992, Detachment faults: Evidence for a low-angle origin: Geology, v. 20, p. 833–836.

Shackelford, T. J., 1980, Tectonic denudation of a Mesozoic-early Tertiary(?) gneiss complex, Rawhide Mountains, western Arizona: Geology, v. 8, p. 190–194.

Spear, F. S., 1993, Metamorphic phase equilibria and pressure-temperature-time paths: Mineralogical Society of America Monograph, 799 p.

Spencer, J. E., 1989, Compilation geologic map of the Buckskin and Rawhide Mountains, west-central Arizona, *in* Spencer, J. E., and Reynolds, S. J., eds., Geology and mineral Resources of the Buckskin and Rawhide Mountains, west-central Arizona: Arizona Geological Survey Bulletin, v. 198, plate 3, scale 1:100 000, 1 sheet.

Spencer, J. E., and Reynolds, S. J., 1989, Tertiary structure, stratigraphy and tectonics of the Buckskin Mountains, *in* Spencer, J. E., and Reynolds, S. J., eds., Geology and mineral resources of the Buckskin and Rawhide Mountains, west-central Arizona: Arizona Geological Survey Bulletin, v. 198, p. 103–167.

Spencer, J. E., and Reynolds, S. J., 1990, The geology and mineral resources of the Bouse Hills, west-central Arizona: Arizona Geological Survey Open-File Report 90–9, scale 1:24 000.

Spencer, J. E., and Reynolds, S. J., 1991, Tectonics of mid-Tertiary extension along a transect through west-central Arizona: Tectonics v. 10, p. 1204–1221.

Spencer, J. E., and Reynolds, S. J., 1994, Stratigraphy of middle Tertiary rocks in the central and eastern Buckskin Mountains, west-central Arizona, *in* Sherrod, D. R., and Nielson, J. E., eds., Tertiary stratigraphy of highly extended terranes, California, Arizona, and Nevada: U.S. Geological Survey Bulletin 2053, p.149–150.

Spencer, J. E., and Welty, J. W., 1986, Possible controls of base- and precious-metal mineralization associated with Tertiary detachment faults in the lower Colorado River trough: Arizona and California: Geology, v. 14, p. 195–198.

Spencer, J. E., Shafiqullah, M., Miller, R. J., and Pickthorn, L. G., 1989a, K-Ar geochronology of Miocene extension, volcanism and potassium metasomatism in the Buckskin and Rawhide Mountains, *in* Spencer, J. E., and Reynolds, S. J., eds., Geology and mineral resources of the Buckskin and Rawhide Mountains, west-central Arizona: Arizona Geological Survey Bulletin, v. 198, p. 168–183.

Spencer, J. E., Grubensky, M. J., Duncan, J. T., Shenk, J. D., Yarnold, J. C., and Lombard, J. P., 1989b, Geology and mineral deposits of the central Artillery Mountains, *in* Spencer, J. E., and Reynolds, S. J., eds., Geology and mineral resources of the Buckskin and Rawhide Mountains, west-central Arizona: Arizona Geological Survey Bulletin, v. 198, p. 168–183.

Spencer, J. E., Reynolds, S. J., and Lehman, N. E., 1989c, Geologic map of the Planet–Mineral Hill area, northwestern Buckskin Mountains, west-central Arizona, *in* Spencer, J. E., and Reynolds, S. J., eds., Geology and mineral resources of the Buckskin and Rawhide Mountains, west-central Arizona: Arizona Geological Survey Bulletin, v. 198, plate 3, scale 1:24 000, 1 sheet.

Steiger, R. H., and Jäger, E., 1977, Subcommission on geochronology: Convention on the use of decay constants in geo- and cosmochronology: Earth and Planetary Science Letters, v. 36, p. 359–362.

Stüwe, K., White, L., and Brown, R., 1994, The influence of eroding topography on steady-state isotherms, application to fission track analysis: Earth and Planetary Science Letters, v. 124, p. 63–74.

Suneson, N. H., and Lucchitta, I., 1979, K-Ar ages of Cenozoic volcanic rocks, west-central Arizona: Isochron/West, no. 24, p. 25–29.

Suneson, N. H., and Lucchitta, I., 1983, Origin of bimodal volcanism, southern Basin and Range province, west-central Arizona: Geological Society of America Bulletin, v. 94, p. 1005–1019.

Wernicke, B. P., and Axen, G. J., 1988, On the role of isostasy in the evolution of normal fault systems: Geology, v. 16, p. 848–851.

Wilkins, J., Jr., and Heidrick, T. L., 1982, Base and precious metal mineralization related to low-angle tectonic features in the Whipple Mountains, California and the Buckskin Mountains, Arizona, *in* Frost, E. G., and Martin, D. L., eds., Mesozoic-Cenozoic tectonic evolution of the Colorado River region, California, Arizona, and Nevada: San Diego, California, Cordilleran Publishers, p. 182–203.

Winslow, D. M., Zeitler, P. K., Chamberlain, C. P., and Hollister, 1994, Direct evidence for a steep geotherm under conditions of rapid denudation, Western Himalaya, Pakistan: Geology, v. 22, p. 1075–1078.

Wooden, J. L., and Miller, D. M., 1990, Chronologic and isotopic framework for early Proterozoic crustal evolution in the eastern Mojave Desert region, SE California: Journal of Geophysical Research, v. 95, p. 133–146.

Woodward, R. J., and Osborne, G. M., 1980, Low-angle detachment faulting and multiple deformation of the central Buckskin Mountains, Yuma County, Arizona: Geological Society of America Abstracts with Programs, v. 12, p. 160.

Wortho, J-A., 1994, Apparent diffusive loss $^{40}Ar/^{39}Ar$ age profiles in amphiboles: Geochronology, Cosmochronology and Isotope Geology Eighth International Conference Abstracts, p. 350.

Wright, J. E., Anderson, J. L., and Davis, G. A., 1986, Timing of plutonism, mylonitization and decompression in a metamorphic core complex, Whipple Mountains, California: Geological Society of America Abstracts with Programs, v. 18, p. 201.

Yarnold, J. C., 1994, Tertiary sedimentary rocks associated with the Harcuvar core complex in Arizona (U.S.A.): Insights into paleogeographic evolution during displacement along a major detachment fault system: Sedimentary Geology, v. 89, p. 43–63.

MANUSCRIPT RECEIVED BY THE SOCIETY NOVEMBER 25, 1996
REVISED MANUSCRIPT RECEIVED AUGUST 25, 1997
MANUSCRIPT ACCEPTED SEPTEMBER 24, 1997

Printed in U.S.A.